ACS Partner Journal

Journal of the American Society for Mass Spectrometry

pubs.acs.org/jasms

Research Article

The DNA Radical Code. Resolution of Identity in Dissociations of Trinucleotide Codon Cation Radicals in the Gas Phase

Jiahao Wan, Břetislav Brož, Yue Liu, Shu R. Huang, Aleš Marek,* and František Tureček*

Cite This: *J. Am. Soc. Mass Spectrom.* 2023, 34, 304−319

Read Online

ACCESS | Metrics & More | Article Recommendations | Supporting Information

ABSTRACT: Sixty DNA trinucleotide cation radicals covering a large part of the genetic code alphabet were generated by electron transfer in the gas phase, and their chemistry was studied by collision-induced dissociation tandem mass spectrometry and theoretical calculations. The major dissociations involved loss of nucleobase molecules and radicals, backbone cleavage, and cross-ring fragmentations that depended on the nature and position of the nucleobases. Mass identity in dissociations of symmetrical trinucleotide cation radicals of the $(XXX+2H)^{+\bullet}$ and $(XYX+2H)^{+\bullet}$ type was resolved by specific ^{15}N labeling. The specific features of trinucleotide cation radical dissociations involved the dominant formation of $\boldsymbol{d}_2^+$ ions, hydrogen atom migrations accompanying the formation of $(\boldsymbol{w}_2+H)^{+\bullet}$, $(\boldsymbol{w}_2+2H)^+$, and $(\boldsymbol{d}_2+2H)^+$ sequence ions, and cross-ring cleavages in the 3′- and 5′-deoxyribose moieties that depended on the nucleobase type and its position in the ion. Born−Oppenheimer molecular dynamics (BOMD) and density functional theory calculations were used to obtain structures and energies of several cation-radical protomers and conformers for $(AAA+2H)^{+\bullet}$, $(CCC+2H)^{+\bullet}$, $(GGG+2H)^{+\bullet}$, $(ACA+2H)^{+\bullet}$, and $(CAA+2H)^{+\bullet}$ that were representative of the different types of backbone dissociations. The ion electronic structure, protonation and radical sites, and hydrogen bonding were used to propose reaction mechanisms for the dissociations.

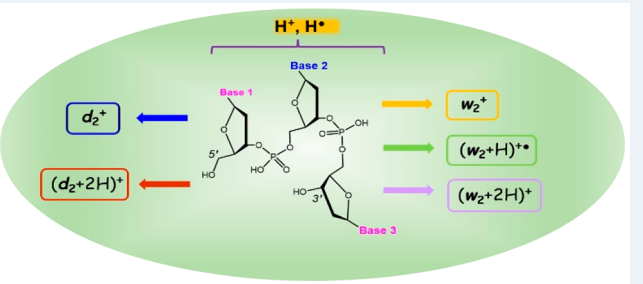

INTRODUCTION

Ionization by high-energy particles or capture of low-energy secondary electrons results in substantial destabilization of the otherwise resistant DNA molecule.[1−4] The major post-ionization processes involve electron[5−12] and proton transfer,[13−16] as well as radical reactions resulting in nucleobase modification,[17−21] loss, or strand breaks.[22,23] While the overall process resulting in DNA damage has been studied extensively with oligonucleotide models, the nature of the reactive intermediates involved in the early stages of DNA ionization only has been investigated with simple nucleosides and small nucleotides.[13−16,24−29] The principal hurdle to experimental structure elucidation of reactive DNA ion radicals has been their very short lifetime in the condensed phase, solution, or frozen glass, where they undergo fast proton transfer reactions with the environment.[24−29] A more recent development in addressing reactive intermediates related to DNA ionization has consisted of generating them in the rarefied gas phase, where side reactions with solvent, oxygen, and other small molecules are avoided. We have generated several neutral nucleobase radicals by femtosecond electron transfer to gas-phase cations and studied their dissociation kinetics and mechanism.[30−34] Major progress in this area has been due to O'Hair and co-workers, who applied collision-induced electron transfer in ternary complexes consisting of Cu(II), terpyridine, and nucleobases to generate cation radicals in an ion trap,[35,36] allowing their further investigation by tandem mass spectrometry[37] and photodissociation action spectroscopy.[38−40] The Cu(II) complex based collision-induced dissociation (CID) method has an inherent limitation in that it excites the complex thermally and nonspecifically, allowing other competitive dissociations to proceed and dominate. Except for the readily oxidizable guanosine and 2′-deoxyguanosine,[38−40] the side reactions have been shown to thwart the formation of even simple nucleoside cation radicals.

A different redox-based method that has been successfully applied to generate oligonucleotide cation radicals in the gas phase relies on ion−ion reactions of multiply protonated oligonucleotides with an electron donor, such as the fluoranthene anion radical that has been used in electron transfer dissociation (ETD).[41] In the nondissociative version of ETD (called ETnoD),[42] the ion−ion reaction results in one-electron reduction but is not accompanied by dissociation. This has been reported for several hexanucleotide[43] and tetranucleotide dications.[44,45] Having access to oligonucleotide cation radicals then makes it possible for one to apply tandem

Received: November 15, 2022
Revised: December 14, 2022
Accepted: December 16, 2022
Published: January 3, 2023

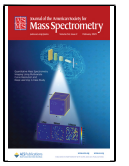

mass spectrometry with CID or UV−vis photodissociation to investigate the cation radical chemistry and electronic structure, as reviewed recently.[46] We now report the results of a comprehensive study of trinucleotide cation-radical dissociations covering a large part of sequences comprising the genetic code alphabet for amino acids in proteosynthesis. Our interest was in identifying the main dissociation types of these cation radicals and their relationship to the trinucleotide sequence and electronic structure. Previous comprehensive studies of trinucleotide mono- and dications[47,48] elucidated the tendency for position and base-specific nucleobase loss and phosphate backbone cleavage occurring between the 5′- and middle position, unambiguously forming $\boldsymbol{w}_2^+$ fragment ions. We now wish to show that dissociations of trinucleotide cation radicals display a much richer chemistry regarding backbone cleavage, proton and hydrogen atom transfer reactions, and 5′- and 3′-deoxyribose cross-ring cleavages. To resolve identity in dissociations of symmetrical trinucleotide cation radicals of the $(XXX + 2H)^{+\bullet}$ and $(XYX + 2H)^{+\bullet}$ type, we apply a set of synthetic trinucleotides specifically labeled with ^{15}N in one of the nucleobases.[49]

EXPERIMENTAL SECTION

Materials and Methods. Custom-made trinucleotides (95% pure) were purchased from Integrated DNA Technologies, Inc. (Coralville, IA), as reported previously.[48] ^{15}N-labeled trinucleotides were manually synthesized on a 200 nmol scale as reported.[49] Dibenzo-18-crown-6-ether (DBCE), 6,7,9,10,17,18,20,21-octahydrodibenzo[*b*,*k*]-[1,4,7,10,13,16]-hexaoxacyclooctadecine, was purchased from Sigma-Aldrich (St. Louis, MO).

Methods. All mass spectra were obtained on a Bruker amaZon 3D-ion trap tandem mass spectrometer (Bruker Daltonik, GmbH, Bremen, Germany) equipped with an auxiliary chemical ionization source for proton transfer and electron transfer dissociations.[50] Electrospray ionization was performed in acetonitrile−water−acetic acid solutions at 50:50:1 component ratios and 10−20 μM concentration of the unlabeled trinucleotides and DBCE. The ^{15}N-labeled trinucleotides that were only available in nmol quantities were dissolved in 1 mL of the solvent mixture, and the solutions were electrosprayed as described previously.[48] Mass-selected doubly charged ions were subjected to ion−ion reactions with fluoranthene anion radicals (ETD-MS^2, 150 ms), and the cation radicals formed were selected for collision-induced dissociation (CID-MS^3). The typical excitation amplitude was 0.4−0.5 on the instrument scale to achieve >60% dissociation of the selected precursor cation radical. A few cation radicals derived from GAA and GCG required a 0.6 amplitude setting to achieve >60% dissociation.

Calculations. Structures of multiple protomers and conformers of trinucleotide cation radicals, $(AAA + 2H)^{+\bullet}$, $(GGG + 2H)^{+\bullet}$, $(CCC + 2H)^{+\bullet}$, $(ACA + 2H)^{+\bullet}$, and $(CCA + 2H)^{+\bullet}$, were obtained by combining Born−Oppenheimer molecular dynamics (BOMD) with density functional theory calculations in the spin-unrestricted format. Initial structures were generated for combinations of low-energy protomers at adenine (protonation at N1, N3, and N7), guanine (protonation at N7), and cytosine (protonation at N3 and O2). Thymine protonation was not considered according to the previous analysis of thymine-rich trinucleotide mono- and dications.[48] BOMD trajectories for each cation-radical protomer were run for 20 ps in 1 fs steps using the Berendsen thermostat[51] with the temperature set at 510 K. BOMD was run with the hybrid semiempirical PM6-D3H4 method[52] including corrections for hydrogen bonds and dispersion interactions. PM6-D3H4 calculations were run with MOPAC[53] under the high-level Cuby4 platform.[54] Since BOMD includes both nuclear and valence-electron motion, the initial proton and hydrogen atom positions were not fixed and could migrate among accessible positions in the same or another nucleobase or phosphate oxygens. Two hundred snapshots were extracted at regular intervals from each 20000-step trajectory, and their geometries were gradient-optimized with PM6-D3H4. The resulting structures were sorted out to remove duplicates, and 15−20 structures were fully gradient optimized with B3LYP[55] and the 6-31G(d,p) basis set, which was complemented by empirical dispersion corrections with Becke−Johnson damping (GD3-BJ).[56] The local energy minima and saddle points were confirmed by harmonic frequency calculations giving the proper number of imaginary frequencies (0 and 1, respectively). Harmonic frequencies calculated by B3LYP-GD3BJ/6-31G(d,p) showed a tight correlation with the more usual B3LYP/6-31+G(d,p) frequencies with a 0.9921 slope, giving a correlation coefficient of r^2 = 0.9999 and root-mean square deviation of rmsd = 1.1 cm^{-1}. Several B3LYP-GD3BJ-optimized low-energy structures were further subjected to reoptimization with M06-2X[57] and the 6-31+G(d,p) basis set, and these structures were used for single-point energy calculations with M06-2X/6-311++G-(2d,p). All relative energies reported here are based on M06-2X/6-311++G(2d,p) calculations including scaled B3LYP-GD3BJ/6-31G(d,p) zero-point vibrational energies, enthalpies, and entropies. The reported thermodynamic data refer to 310 K, which is the ion trap ambient temperature. Previous benchmarking of M06-2X/6-311++G(2d,p) relative energies versus those calculated by coupled cluster methods for nucleobase and nucleoside cation radicals showed a close correlation and identical energy ranking for both sets.[58] Atomic charges and spin densities were obtained from natural population analysis[59] (NPA) calculations with M06-2X/6-311++G(2d,p). These standard calculations were performed with the Gaussian 16 suite of programs, Revision B.01, licensed from Gaussian, Inc. (Wallingford, CT).

RESULTS AND DISCUSSION

Generation of Codon Cation Radicals. The cation radicals were prepared from mass-selected dications obtained by electrospray ionization that were subjected to reduction by electron transfer in ion−ion reactions with fluoranthene anions. The electron transfer was calculated to be highly exothermic ($\Delta H_{rxn} < -580$ kJ mol^{-1}), resulting in a substantial dissociation (ETD) of the formed cation radicals. This is illustrated with $(AGC+2H)^{2+}$ (m/z 435.5, Figure 1a) that upon electron transfer showed loss of cytosine, 3′-cross-ring cleavages, and backbone dissociation forming the $\boldsymbol{d}_2$ ion at m/z 661. More seriously, ETD of codon dications also resulted in deprotonation, forming monocations, such as $(AGC+H)^+$ at m/z 870 (Figure 1a, inset). This side reaction was of concern, because the monocations from the various combinations of nucleosides carried along 33−39% of combined natural ^{13}C and ^{15}N isotopologues that overlapped by mass with the cation radicals. The isotope satellites were difficult to remove by narrowing the mass selection window for the dications because of reduced ion intensity. To improve the formation of codon cation radicals, we used ETD of doubly charged noncovalent

https://doi.org/10.1021/jasms.2c00322
J. Am. Soc. Mass Spectrom. 2023, 34, 304−319

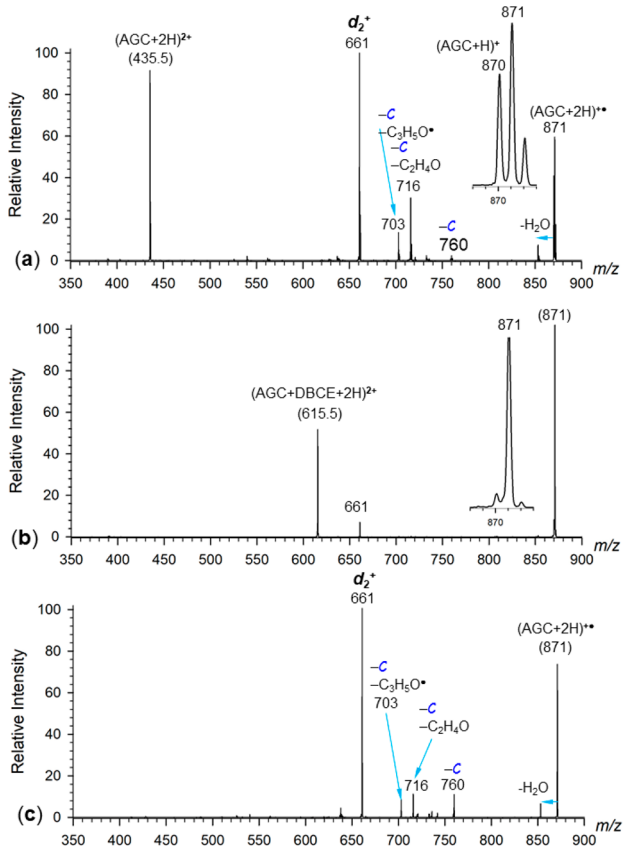

Figure 1. ETD-MS^2 spectra of (a) $(AGC+2H)^{2+}$ at m/z 435.5 and (b) noncovalent complex with dibenzo-18-crown-6-ether, $(AGC+DBCE+2H)^{2+}$, at m/z 615.5. (c) CID-MS^3 spectrum of $(AGC+2H)^{+\bullet}$ at m/z 871 that was mass-isolated from the spectrum in (b). Insets in (a) and (b) show the peak profiles of the charge-reduced ions.

complexes of trinucleotides with dibenzo-18-crown-6-ether (DBCE),[60−62] as shown for the $(AGC+DBCE+2H)^{2+}$ ion, m/z 615.5 (Figure 1b). Complexation with crown ethers such as DBCE has been shown to lower the recombination energy of the dication, thus reducing the electron transfer exergonicity.[63] For example, the recombination energies of dAA dinucleotide dications have been shown to drop from 617 to 485 kJ mol^{-1} in the DBCE complex.[60] DBCE binding to the trinucleotide ion is greatly reduced upon reduction, chiefly due to weaker hydrogen bonds to the nucleobase radical.[63] In addition, the departing DBCE carries away a fraction of the ET-generated excitation energy, which has been estimated to be roughly proportional to the number of degrees of freedom of the products.[64] For the trinucleotide complexes, DBCE was estimated to retain 32−35% of internal energy after ETD, aiding trinucleotide cation radical stabilization. These combined effects in complex reduction and expulsion of the crown ether resulted in a very clean production of trinucleotide cation radicals, such as $(AGC+2H)^{+\bullet}$ at m/z 871, showing less dissociation and virtually no deprotonation. Interestingly, the formation of $(AGC+H)^+$ upon ETD of naked codon dications was entirely due to proton transfer in the ion−ion reaction, and not loss of a hydrogen atom from the cation radicals, as previously discussed for peptide cation radicals.[65] This was corroborated by the CID-MS^3 spectra of the codon cation radicals, such as that of $(AGC+H)^{+\bullet}$ (Figure 1c), which showed no loss of hydrogen. DBCE complexes were used to generate all cation radicals that showed substantial deprotonation accompanying electron transfer reduction, in particular those from AGC, CAC, CCC, CGC, and CTC. The CID-MS^3 spectra of the cation radicals showed fragment ions arising by loss of a nucleobase and backbone dissociations leading to $\boldsymbol{d_2}^+$ and $\boldsymbol{w_2}^+$ ions. In addition, hydrogen transfer reactions were observed, resulting in the loss of nucleobase radicals, primarily GH$^\bullet$, and formation of $(\boldsymbol{w_2} \pm n\mathrm{H})^{+\bullet}$ and $(\boldsymbol{d_2} + 2\mathrm{H})^+$ ions. These reactions depended on the nature and position of the nucleobases in the codon cation radical. The dissociations were resolved by ^{15}N labeling, as described systematically below for the different nucleotide sequences.

Note on Nomenclature. We use the traditional nomenclature of DNA fragment ions that has been established for even-electron ions.[66−68] Thus, $\boldsymbol{a_n}^+$, $\boldsymbol{d_n}^+$, and $\boldsymbol{w_n}^+$ even-electron ions correspond by mass to neutral molecular fragments from backbone phosphate ester cleavage with an attached proton at a nucleobase. Radical cations having the m/z one unit higher or lower than $\boldsymbol{a_n}^+$ and $\boldsymbol{w_n}^+$ are denoted as $(\boldsymbol{a_n} \pm \mathrm{H})^{+\bullet}$ $(\boldsymbol{w_n} \pm \mathrm{H})^{+\bullet}$, respectively. Other differences in the hydrogen atom count are expressed by $\pm n$H added to the fragment ion symbol.

Backbone Dissociation Types in Trinucleotide Cation Radicals. Standard backbone cleavages in trinucleotides by phosphate ester elimination can result in the formation of $\boldsymbol{d_2}^+$ ions retaining the 5′- and middle nucleobases or $\boldsymbol{w_2}^+$ ions retaining the 3′- and middle nucleobases.[47,48,66−68] With hydrogen-rich cation radicals containing an additional hydrogen atom in the radical-carrying nucleobase, one also observes backbone dissociations that are associated with hydrogen atom transfer, forming odd-electron $(\boldsymbol{w_2}+\mathrm{H})^{+\bullet}$ and even-electron $(\boldsymbol{w_2}+2\mathrm{H})^+$ and $(\boldsymbol{d_2}+2\mathrm{H})^+$ ions. The main types of dissociation by nucleobase loss, phosphate ester backbone cleavage, and cross-ring fragmentations for 60 codon trinucleotide cation radicals are summarized in the master table (Table 1). To illustrate and detail other ion fragmentations, full CID-MS^3 spectra are also shown in Figures S1−S12 in the Supporting Information.

The $\boldsymbol{d_2}^+$ Ion Group. The largest group of trinucleotide cation radicals displayed CID-MS^3 spectra with dominant $\boldsymbol{d_2}^+$ backbone fragment ions, arising by a combined loss of the 3′-nucleobase and a $C_5H_7O_2$ radical from the 3′-deoxyribose moiety while the charging proton was retained at the 5′- or middle nucleotides. Codon cation radicals undergoing major dissociation to $\boldsymbol{d_2}^+$ ions included the following sequences: AAC, ACC, AGC, ATC, CAC, CGC (Figure S1a−f), AAT, AGA, [^{15}N$_5$]AGA, ATT, ATA, [^{15}N$_5$]ATA, (Figure S2a−f), GCC, CTC, AGT, GGC, GAC, GTC (Figure S3a−f), and CCC, [^{15}N$_3$]CCC, TCC, TAA, TAC, and TGC (Figure S4a−g). The majority of these sequences shared two structural features. (1) There was a basic (A or G) nucleobase in the 5′-, middle or both positions to sequester the charging proton in the $\boldsymbol{d_2}^+$ ion. (2) The 3′-base was a pyrimidine, C or T, with the exception of AGA, ATA, and TAA. We note that these last three cation radicals also underwent other backbone cleavages; thus, the preference for the $\boldsymbol{d_2}^+$ ion formation was not so prevalent. The formation of $\boldsymbol{d_2}^+$ ions can be explained by the reaction sequence generically shown in Scheme 1. One-electron transfer to the precursor dication resulted in the formation of a radical at the 3′-nucleobase. This can occur by direct reduction of a protonated 3′-cytosine, or by hydrogen atom transfer from the reduced 5′- or middle nucleobase onto 3′-cytosine or thymine. We note that pyrimidine nucleobases

https://doi.org/10.1021/jasms.2c00322
J. Am. Soc. Mass Spectrom. 2023, 34, 304−319

Table 1. CID-MS^3 Spectra

sequence[a]	base loss	backbone fragments	cross-ring loss
AAA	5′ > 3′ > middle (52:42:6)	w_2^+ > d_2^+ (54:46)	
AAC	*C* > *A*	d_2^+	
AAG	*A* > *G*, GH$^\bullet$	$w_2^+ \approx (w_2+H)^{+\bullet}$ > d_2^+	
AAT	*A* > *T*	$d_2^+ \gg w_2^+$, $(w_2+H)^{+\bullet}$, $(w_2+2H)^+$	(*T*+C_2H_4O, C_3H_5O)
ACA	5′-*A* ≈ 3′-*A*, *C*	$(d_2+2H)^+$ > $(w_2+2H)^+$ (67:33)	
ACC	*C* ≫ *A*	d_2^+	
ACG	*C* > *G*, GH$^\bullet$, *A*	$(d_2+2H)^+ \approx (w_2+2H)^+ > (w_2+H)^{+\bullet}$, $(z_2+H)^{+\bullet}$	
ACT	*C* > *A*	$(z_2+H)^{+\bullet}$, $(w_2+2H)^+ > (d_2+2H)^+ > d_2^+$,	
AGA	3′-*A* > 5′-*A*, *C*	$d_2^+ > w_2^+ > (w_2+H)^{+\bullet}$	(*A*+C_2H_4O, C_3H_5O)
AGC	*C*	d_2^+	(*C*+C_2H_4O, C_3H_5O)
AGG	*G* > *A*	$(w_2+H)^{+\bullet} > d_2^+$, $(a_2-H)^{+\bullet}$	(*G*+C_2H_4O, C_3H_5O)
AGT	*A* ≈ *G*	$d_2^+ > (w_2+H)^{+\bullet} > w_2^+$	(*T*+C_2H_4O, C_3H_5O)
ATA	5′-*A* ≈ 3′-*A*	$d_2^+ > w_2^+ > (w_2+H)^{+\bullet}$	
ATC	*C* ≫ *A*	$d_2^+ \gg (w_2+H)^{+\bullet}$	(*C*+C_2H_4O, C_3H_5O)
ATG	*A* > *G*	$(w_2+H)^{+\bullet} > w_2^+ > d_2^+$	
ATT	*A* ≈ *T*	$d_2^+ > w_2^+$, $(a_2-H)^{+\bullet}$	(*T*+C_3H_5O)
CAA	*C*	w_2^+	$CH_2OH^\bullet$
CAC	*A*	d_2^+, d_2^+-C	
CAG	*C*	$w_2^+ > (w_2-H)^{+\bullet} > (w_2+H)^{+\bullet}$	$CH_2OH^\bullet$
CAT	*C*	$w_2^+ > (w_2+H)^{+\bullet}$	$CH_2OH^\bullet$
CCA	*C*	$(d_2+2H)^+ > w_2^+$	$CH_2OH^\bullet$
CCC	3′ > 5′ ≈ middle > CH$^\bullet$ 90:05:05	$d_2^+ > (d_2+2H)^+$	(*C*+C_2H_4O, C_3H_5O)
CCG	*G*$^\bullet$ > *C*	$(d_2+2H)^+ \approx (w_2-H)^{+\bullet} > w_2^+ > (w_2+2H)^+$	$CH_2OH^\bullet$
CCT	*C*	$w_2^+ \gg (w_2+H)^{+\bullet}$	$CH_2OH^\bullet$
CGA	*C* ≫ *A*	$w_2^+ > (w_2-H)^{+\bullet} \approx (w_2+H)^{+\bullet}$	$CH_2OH^\bullet$
CGC	5′-*C* > 3′-*C*, *G*$^\bullet$	d_2^+	(3′-C+C_2H_4O)
CGG	*C* ≈ *G*	$(w_2-H)^{+\bullet} > (w_2+H)^{+\bullet} > w_2^+$	$CH_2OH^\bullet$
CTA	*C*	w_2^+	$CH_2OH^\bullet$
CTC	3′-*C* > *T*$^\bullet$	$d_2^+ > (d_2-H)^{+\bullet}$	
CTG	*C* > *G*	$w_2^+ > (w_2+H)^{+\bullet} > (w_2-H)^{+\bullet}$	$CH_2OH^\bullet$
CTT		$d_2^+ \approx w_2^+$	$CH_2OH^\bullet$
GAA	*A* > *G*, GH$^\bullet$, GH_2	$w_2^+ > (w_2+H)^{+\bullet} \approx d_2^+$	
GAC	*G* > *C*	$d_2^+ > (w_2+H)^{+\bullet} > w_2^+$	(*C*+C_2H_4O, C_3H_5O)
GAG	5′-*G* > 3′-*G*	$(w_2+H)^{+\bullet} > w_2^+ \gg d_2^+$	
GAT	GH$^\bullet$ > *G*	$w_2^+ > w_2+H)^{+\bullet} > d_2^+$	
GCA	*G* > *C*	$(d_2+2H)^+ > (w_2+H)^{+\bullet} > w_2^+$	
GCC	*G* > *C*	$d_2^+ \gg (w_2+2H)^+$	(*C*+C_2H_4O, C_3H_5O)
GCG	5′-*G* > 3′-*G* > 3′-GH$^\bullet$	$(w_2+H)^{+\bullet} > (w_2+2H)^+ > (d_2+2H)^+$	
GCT	*G* > *C*	$(w_2+H)^{+\bullet} > w_2^+$ $(w_2+2H)^+ > (d_2+2H)^+$	
GGA	*G* > *A*, GH$^\bullet$, GH_2	$w_2^+ \approx (w_2+H)^{+\bullet} > d_2^+$	
GGC	*G* > *C*, GH$^\bullet$	d_2^+	(*C*+C_2H_4O, C_3H_5O)
GGG	5′ > 3′ > middle (57:30:13)	$(w_2+H)^{+\bullet} > w_2^+$	
GGT	*G* > GH$^\bullet$	$(w_2+H)^{+\bullet} > w_2^+$	(*T*+C_3H_5O)
GTA	*G* > GH$^\bullet$ > GH_2, *C*	$w_2^+ > (w_2+H)^{+\bullet} > d_2^+$	
GTC	*G* > *C* > *T*$^\bullet$, GH$^\bullet$	$d_2^+ > (w_2+H)^{+\bullet} > w_2^+$	(*C*+C_2H_4O, C_3H_5O)
GTG	5′-*G* > 3′-*G*	$(w_2+H)^{+\bullet} > w_2^+$	
GTT	*G* ≈ *T*	$(w_2+H)^{+\bullet} > w_2^+$	98 Da
TAA	*A*	$d_2^+ > > w_2^+ > (d_2+2H)^+ > (w_2+2H)^+$	$CH_2OH^\bullet$
TAC	*C*	$d_2^+ \gg (w_2+2H)^+$	(*C*+C_2H_4O, C_3H_5O)
TAT		$(w_2/d_2+2H)^+ > w_2/d_2$	(41 Da)
TCA	*C* > *A*	$(d_2+2H)^+ \gg (w_2+2H)^+$	
TCC	*C*	$d_2^+ > (d_2-H)^{+\bullet} \approx (w_2+2H)^+$, $(z_2+H)^{+\bullet}$	
TCG	*C*, *G*	$(w_2+2H)^+ > (d_2+2H)^+$, $(z_2+H)^{+\bullet}$	
TCT		$(w_2/d_2+2H)^+ > w_2/d_2$, $(a_2/z_2+H)^{+\bullet}$	
TGC	*C*	$d_2^+ > (w_2+2H)^+$	(*C*+C_2H_4O, C_3H_5O)
TGG	*G*	$w_2 \approx d_2$	
TGT	*G* > *T*, TH$^\bullet$	$w_2/d_2 > (w_2/d_2+H)^{+\bullet}$	(*T*+C_2H_4O, C_3H_5O)
TTA		$(w_2+2H)^+ > w_2^+$	
TTC		$(w_2+2H)^+ > (w_2-2H)^+$	
TTG		$w_2^+ > (w_2+H)^{+\bullet}$, $(w_2-H)^{+\bullet}$, d_2^+	

https://doi.org/10.1021/jasms.2c00322
J. Am. Soc. Mass Spectrom. 2023, 34, 304−319

Table 1. continued

[a]Sequences for which fragment ion assignments were supported by ^{15}N labeling are shown in boldface.

Scheme 1. Generic Mechanisms for the Formation of d_2^+ Sequence Fragment Ions

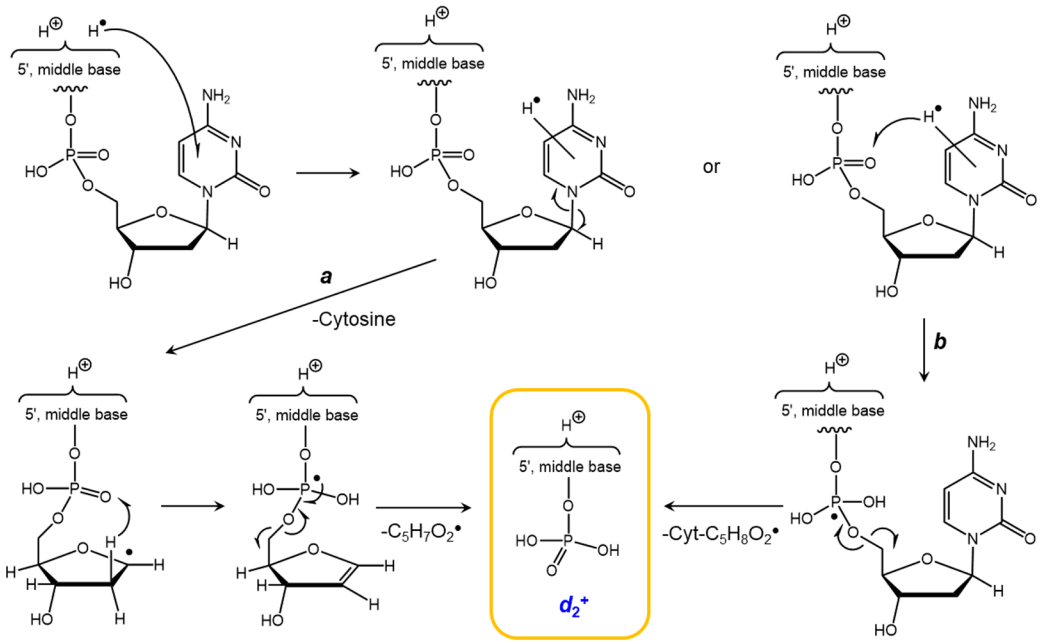

Scheme 2. Generic Mechanisms for the Formation of w_2^+ Sequence Fragment Ions

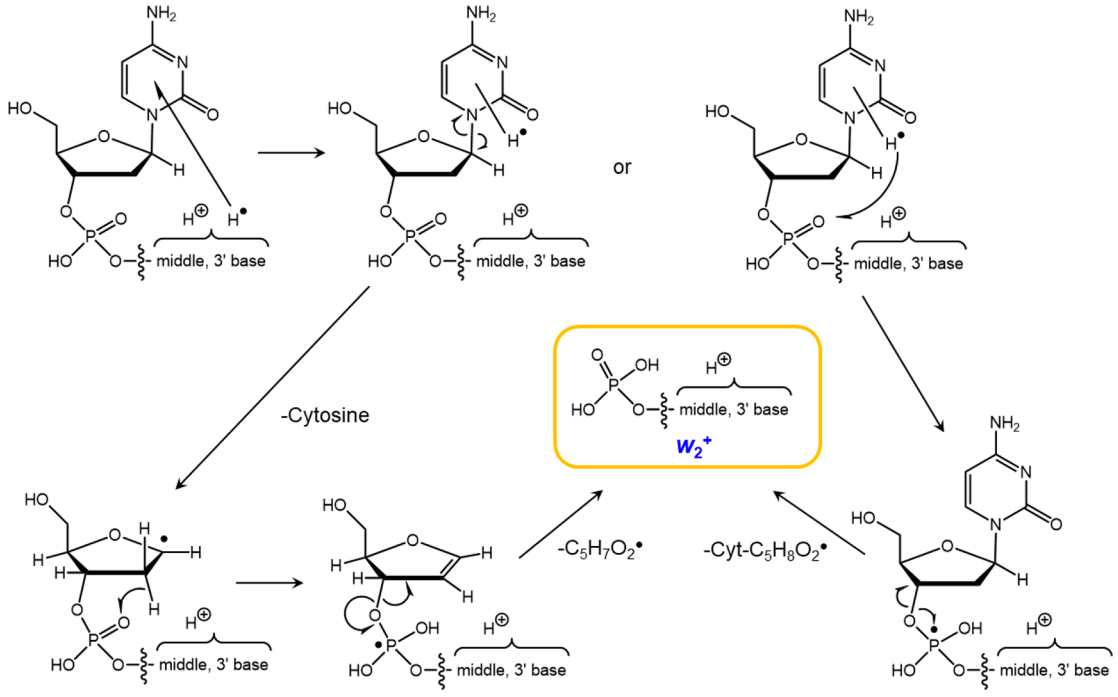

in nucleosides have greater hydrogen atom affinities than purine nucleobases, as studied for nucleobase[69,70] and nucleoside radical conjugates.[61,62] For example, addition of a hydrogen atom at the N3 position in cytosine and 1-methylcytosine has been calculated to be exergonic by 130 kJ mol^{-1} to produce the lowest-energy radical adducts.[69] By comparison, addition of a hydrogen atom to the N1 and C8 positions in adenine was exergonic by 53 and 105 kJ mol^{-1}, respectively.[70] Thus, a hydrogen atom transfer from a purine nucleobase radical to a neutral pyrimidine nucleobase was expected to be exergonic. Hydrogen atom transfer must be the sole mechanism to generate thymine radicals, because the very low thymine basicity in nucleotides prevents it from direct protonation.[48,71] The 3′-nucleobase radical was expected to dissociate by a base loss, forming a C1′-deoxyribose radical (Scheme 1). Previous studies of nucleoside radicals have

https://doi.org/10.1021/jasms.2c00322
J. Am. Soc. Mass Spectrom. 2023, 34, 304−319

indicated that loss of the base was a major dissociation.[61,62] These loss-of-base intermediates were seen in the CID-MS^3 spectra of the cation radicals (Figures S1−S4). The further dissociation could be envisioned as a standard phosphate ester elimination that has been considered for dissociations of oligonucleotide cations.[47,48,68,72] However, this interpretation could not account for the facile formation of d_2^+ ions from the cation radicals in light of the fact that trinucleotide even-electron mono- and dications do not form d_2^+ ions at all.[47,48]

We propose two different mechanisms that take into account the radical nature of the intermediates (Scheme 1). The loss-of-base pathway (*a*) presumes hydrogen atom transfer from the deoxyribose radical onto the phosphate group, followed by homolytic cleavage of the C5′−O bond and loss of the $C_5H_7O_2$ radical, forming the d_2^+ ion. The alternative direct pathway (*b*) includes a hydrogen atom transfer from the nucleobase radical to the phosphate group followed by homolytic cleavage of the C5′−O bond. The phosphate hydrogen atom affinity (37 kJ mol^{-1})[73] indicated that the hydrogen atom migration to the phosphate group should be endergonic and needs to be driven by collisional excitation. These dissociation pathways are more specifically depicted later for (CCC + 2H)$^{+\bullet}$, including fully optimized structures and M06-2X/6-311++G(2d,p) + ZPVE relative and transition-state energies.

The w_2^+ Ion Group. Cation radicals derived from CAA, CTA, CAG, CCT, CAT, CGA (Figure S5a−f) and CTG, GAT, TTG, GAA, GTA, TGT (Figure S6a−f) showed major w_2^+ fragment ions upon CID-MS^3. These dissociations were to some extent accompanied by other backbone cleavages: namely, formation of minor d_2^+ ions (GAA, GAT, GTA) and hydrogen transfers leading to the formation of $(w_2+H)^{+\bullet}$ ions which were observed for CAT, GAA, GTA, and GAT and $(w_2\pm H)^{+\bullet}$ cation radicals seen for CGA and CTG within this group. The formation of w_2^+ necessitates radical-induced fragmentation at the 5′-nucleoside involving a combined loss of the 5′-base and sugar $C_5H_7O_2$ radical and retention of the charging proton at the 3′- or middle nucleobase. The trinucleotides having 5′-cytosine satisfied the first criterion whereby formation of a 5′-cytosine radical was expected to trigger the loss of the base. Similarly, the 5′-guanine base in GAA, GAT, and GAT was likely to be protonated in the precursor dication and converted upon electron attachment into a 5′-guanine radical, thus facilitating 5′-nucleobase loss. Alternatively, w_2^+ ions could be produced by a direct loss of an a_1 neutral radical which was analogous to the formation of d_2^+ ions (Scheme 2).

The $(w_2+H)^{+\bullet}$ Ion Group. Another large group of trinucleotide cation radicals showed prominent formation of backbone $(w_2+H)^{+\bullet}$ fragment ions. The sequences undergoing this dissociation involved AAG, GGA, GGT, GCT, GTT, GCA (Figure S7a−f) and AGG, ATG, CGG, GAG, GCG, GTG (Figure S8a−f). A common feature of these sequences was that they all contained guanine and most also contained another basic purine nucleobase. GTT was an obvious exception, with the caveat that double protonation of this sequence was very inefficient, resulting in weak doubly charged ions and hence also a low-quality ETD spectrum for CID-MS^3. We note that thymine protonation in trinucleotides is energetically disfavored, so that the second proton in the $(GTT+2H)^{2+}$ precursor dication could be attached to one of the phosphate ester oxygens,[48] thus affecting the structure and chemistry of $(GTT+2H)^{+\bullet}$ following electron transfer. The formation of $(w_2+H)^{+\bullet}$ ions can be viewed as resulting from a combined loss of the 5′-nucleobase and 5′-deoxyribose in the form of a $C_5H_6O_2$ molecule that involved placing a proton and a hydrogen atom at the middle and 3′-bases in the fragment cation radical. This can be achieved by hydrogen atom or proton transfer from the 5′-nucleoside or proton and H atom retention at the middle and 3′-bases in the initial cation radical structure. A possible mechanism for the $(w_2+H)^{+\bullet}$ fragment ion formation will be shown later for $(GGG+2H)^{+\bullet}$ using fully optimized cation-radical structures and M06-2X/6-311++G-(2d,p) + ZPVE energies.

The $(w_2+2H)^+$ and $(d_2+2H)^+$ Ion Groups. Double hydrogen/proton transfer was observed for dissociations of several trinucleotides. CID-MS^3 of $(ACG+2H)^{+\bullet}$, $(ACT+2H)^{+\bullet}$ (Figure 2a,b), $(TCA+2H)^{+\bullet}$, and $(TCT+2H)^{+\bullet}$,

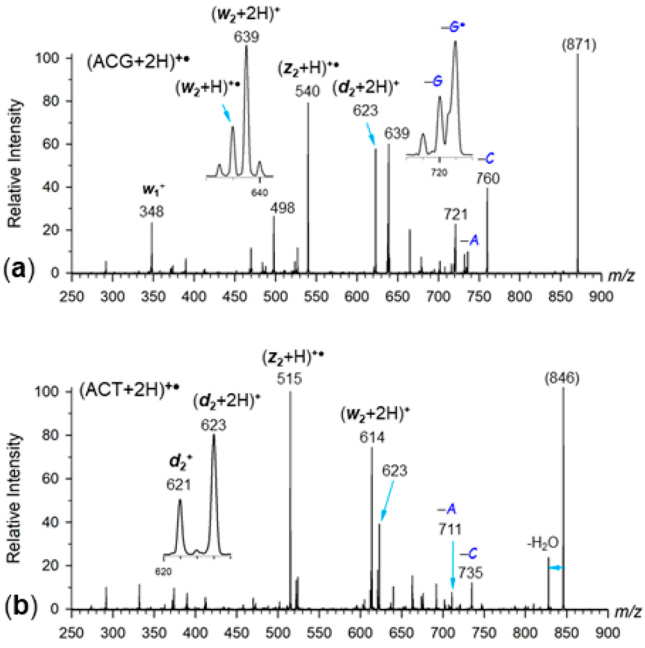

Figure 2. CID-MS^3 spectra of (a) $(ACG+2H)^{+\bullet}$ and (b) $(ACT+2H)^{+\bullet}$. Insets show the fragment peak profiles.

showed prominent $(w_2+2H)^+$ fragment ions (Figure S9), which retained the charging proton and gained additional two hydrogen atoms after loss of the 5′-nucleobase and a $C_5H_5O_2$ radical from 5′-deoxyribose. A common structural feature among the trinucleotide cation radicals undergoing this dissociation was the presence of a purine (C or T) nucleobase in the middle position. The $(w_2+2H)^+$ ions were accompanied by other specific backbone cleavages. For example, $(ACG+2H)^{+\bullet}$ and $(ACT+2H)^{+\bullet}$ showed prominent odd-electron $(z_2+H)^{+\bullet}$ fragment ions indicating cleavage of the phosphate O−C5′ bond at the middle nucleotide (Figure 2a,b). Alternatively, the $(z_2+H)^{+\bullet}$ ions can be formed by phosphoric acid elimination (H_3PO_4, Δm = 98 Da) from the respective $(w_2+H)^{+\bullet}$ ions which also appeared in the CID-MS^3 spectra of these trinucleotide cation radicals (Figure 2). CID-MS^3 of another group of trinucleotide cation radicals, $(ACA+2H)^{+\bullet}$, $(TCA+2H)^{+\bullet}$, $(GCA+2H)^{+\bullet}$, $(CCA+2H)^{+\bullet}$, $(CCG+2H)^{+\bullet}$, and $(TAT+2H)^{+\bullet}$, showed the formation of $(d_2+2H)^+$ fragment ions by a combined loss of the 3′-base and a $C_5H_5O_2$ radical from 3′-deoxyribose (Figure S9). The formation of the $(d_2+2H)^+$ ions coincided with that of

https://doi.org/10.1021/jasms.2c00322
J. Am. Soc. Mass Spectrom. 2023, 34, 304−319

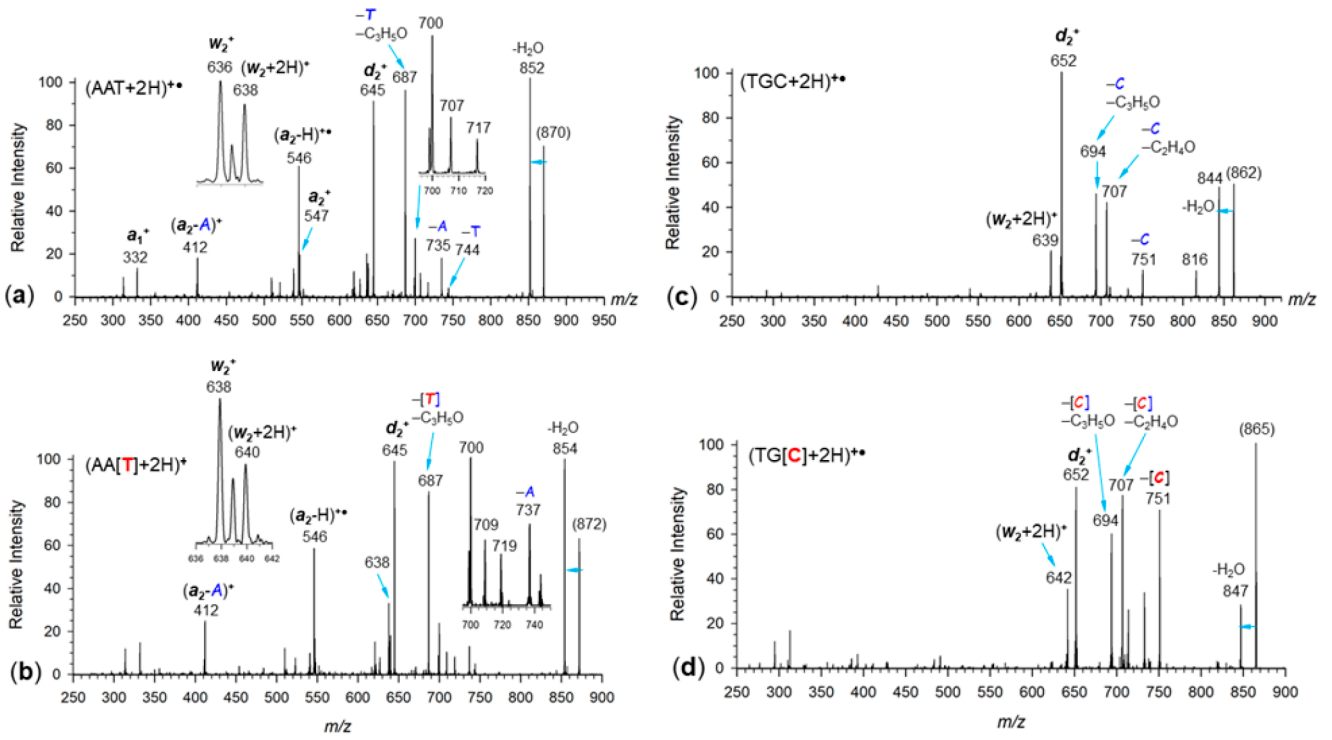

Figure 3. CID-MS^3 spectra of (a) $(AAT+2H)^{+\bullet}$, (b) $(AA[^{15}N_2\text{-}T]+2H)^{+\bullet}$, (c) $(TGC+2H)^{+\bullet}$, and (d) $(TG[^{15}N_3{-}C]+2H)^{+\bullet}$. Insets show the fragment ion peak profiles. The ^{15}N-labeled nucleobases are shown in red in brackets.

Scheme 3. Generic Mechanism for the Loss of CH_2OH

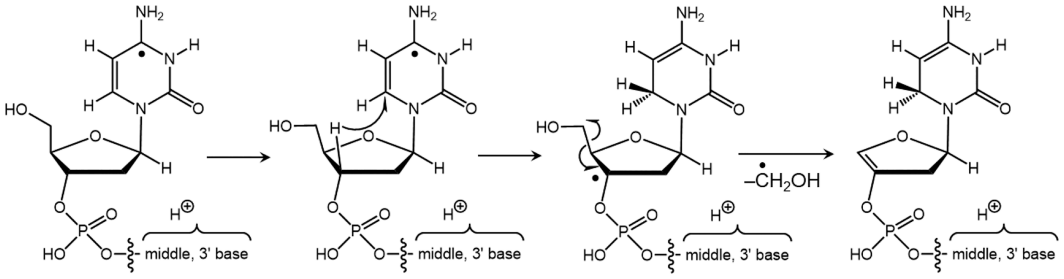

$(\boldsymbol{w}_2{+}2H)^+$, as seen for ACA, GCA, ACG, and TCA, but not CCA, which coformed $\boldsymbol{w}_2^+$ ions instead.

In addition, the $(\boldsymbol{d}_2{+}2H)^+$ ions were accompanied by $\boldsymbol{d}_2^+$ but not $(\boldsymbol{d}_2{+}H)^{+\bullet}$, indicating that the phosphate cleavage between the middle and 3′-nucleoside was always accompanied by loss of a 3′-deoxyribose radical. The consistent feature of the $(\boldsymbol{d}_2{+}2H)^+$-forming trinucleotides was the presence of a cytosine residue as the middle base and loss of a purine (A or G) 3′-nucleobase.

Cross-Ring Dissociations. In addition to undergoing backbone phosphate cleavages, trinucleotide cation radicals having 3′- and 5′- terminal cytosine or thymine showed radical-induced dissociations in the pertinent terminal deoxyribose moieties (Figure 3a–d). Loss of the CH_2OH radical was observed for trinucleotides having 5′-cytosine, as in $(CCT+2H)^{+\bullet}$, $(CCA+2H)^{+\bullet}$, $(CAA+2H)^{+\bullet}$, $(CAT+2H)^{+\bullet}$, $(CTA+2H)^{+\bullet}$, $(CTG+2H)^{+\bullet}$, and $(CGA+2H)^{+\bullet}$, but much less so or not at all in $(CCC+2H)^{+\bullet}$, $(CAC+2H)^{+\bullet}$, $(CGC+2H)^{+\bullet}$, and $(CTC+2H)^{+\bullet}$. The latter group of cation radicals was found to produce abundant $\boldsymbol{d}_2^+$ ions which presumably outcompeted dissociations in the 5′-deoxyribose ring. The loss of the CH_2OH radical is likely to be initiated by a hydrogen atom transfer within the 5′-deoxyribose ring to weaken the C4′–C5′ bond, as tentatively shown in Scheme 3.

The spectra of cation radicals undergoing CH_2OH radical loss also showed prominent fragment ions by the competitive loss of cytosine. This indicated that these dissociations were promoted by the formation of a 5′-cytosine hydrogen atom adduct upon electron transfer. Compared to the above group, trinucleotide cation radicals having 5′-thymine underwent less frequent loss of $^{\bullet}CH_2OH$, as illustrated with $(TAA+2H)^{+\bullet}$ (Figure S4e in the Supporting Information).

Cytosine and thymine residues at the 3′-terminus showed still different cross-ring dissociations in the 3′-deoxyribose moiety, resulting in the combined loss of the 3′-base and a C_2H_4O molecule or a $C_3H_5O^{\bullet}$ radical. This was observed for AAT, ATT, AGT, GAT, CAT, GGC, GAC, AGC, GTC, GCC, CGC, TGC, TGT, and TAC. The origin of these fragment ions was corroborated by ^{15}N labeling in $AA[^{15}N_2\text{-}T]$ and $TG[^{15}N_3{-}C]$ (Figure 3b,d). The spectrum of $AA[^{15}N_2\text{-}T]$ showed retention of the m/z 687 fragment ion (Figure 3b) for the loss of $([^{15}N_2\text{-}T] + C_3H_5O)$ (Figure 3b). Similarly, $TG[^{15}N_3{-}C]$ showed retention of m/z 707 and m/z 694 upon combined elimination of 3′-cytosine, C_2H_4O, and $C_3H_5O^{\bullet}$,

https://doi.org/10.1021/jasms.2c00322
J. Am. Soc. Mass Spectrom. 2023, 34, 304–319

Scheme 4. Generic Mechanisms for Cross-Ring Cleavages

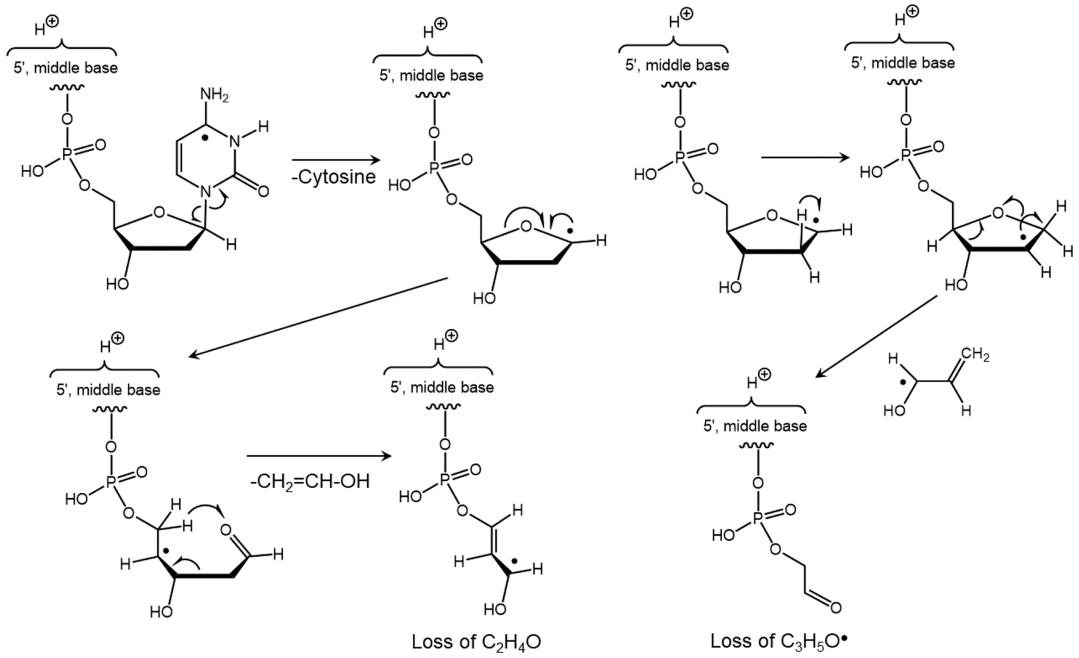

respectively (Figure 3d). Because of the nature of these dissociations, it was plausible to propose a mechanism starting from a radical intermediate produced by the loss of the 3′-nucleobase, as shown for cytosine in Scheme 4. The C1′-radical at the 3′-sugar can undergo ring opening by cleavage of the C4′−O bond forming a C4′ radical. Hydrogen transfer to the newly formed aldehyde carbonyl is followed by cleavage of the C2′−C3′ bond and elimination of C_2H_4O as vinyl alcohol. The competing loss of $C_3H_5O^{\bullet}$ can be presented as starting by hydrogen 1,2-migration bringing the radical at C2′ and facilitating homolytic cleavage of the C1′−O bond and forming an allylic C1′−C2′−C3′ system in the intermediate oxide radical. This was be expected to undergo a facile dissociation of the C4′−C3′ bond, leading to the loss of $CH_2{=}CH{-}CHOH$ radical. It should be noted that the dissociation leading to the loss of $(T+C_3H_5O)$ from trinucleotide cation radicals containing 3′-thymine may proceed by a radical-induced deoxyribose ring cleavage directly in the trinucleotide cation radicals. This is indicated by the very low propensity for the loss of thymine hindering the formation of the pertinent deoxyribose radical intermediates.

Resolution of Identity in Dissociations of $(AAA+2H)^{+\bullet}$, $(CCC+2H)^{+\bullet}$, and $(GGG+2H)^{+\bullet}$. Loss of the nucleobase was the primary dissociation observed in the CID-ETD-MS^3 spectra of all three symmetrical codon cation radicals (Figure 4a−c). In addition to the loss of nucleobase molecules, the spectra also showed a minor loss of nucleobase radicals as neutral hydrogen adducts $AH^{\bullet}$, $CH^{\bullet}$, and $GH^{\bullet}$. The formation of these radicals must have involved hydrogen atom migration to the nucleobase radical produced by electron transfer reduction of the protonated nucleobase. The positional identity for the nucleobase loss was resolved by ^{15}N labeling as shown in Figures S10−S12 in the Supporting Information. With $(AAA+2H)^{+\bullet}$, where we had a complete set of 5′-, middle, and 3′-$^{15}N_5$-labeled codons, the distribution was 54:8:38 for the loss of the nucleobase from the corresponding positions. This was similar to the loss of adenine from $(AAA+H)^{+}$ cations,[48] indicating that the presence of the adenine

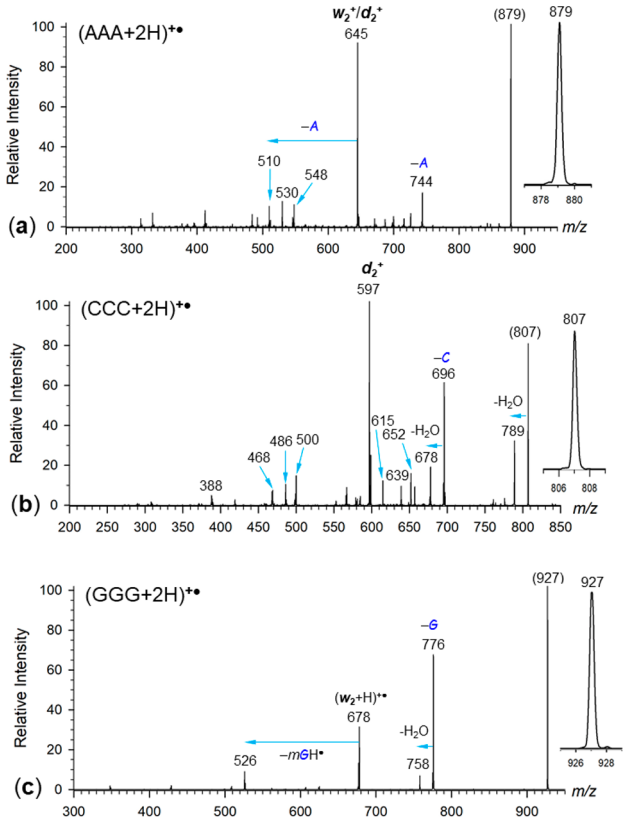

Figure 4. CID-MS^3 spectra of (a) $(AAA+2H)^{+\bullet}$ (m/z 879), (b) $(CCC+2H)^{+\bullet}$ (m/z 807), and (c) $(GGG+2H)^{+\bullet}$ (m/z 927) ions. Insets show the precursor ion peak profiles. See text for fragment ion assignment.

radical did not have a major effect on this base distribution. Loss of cytosine from $(CCC+2H)^{+\bullet}$ was resolved to show an 8:12:80 ratio for the loss of the 5′-, middle, and 3′-nucleobase. This was slightly more biased toward the loss of the 3′-nucleobase compared to the dissociations of the $(CCC+H)^{+}$

https://doi.org/10.1021/jasms.2c00322
J. Am. Soc. Mass Spectrom. 2023, 34, 304−319

cations.[48] With $(GGG+2H)^{+\bullet}$ we observed a 66:11:23 ratio for the loss of the 5′-, middle, and 3′-guanine, which represented a broader distribution of positions compared to that for the dissociations of $(GGG+H)^{+}$ cations.[48] We note that $(TTT+2H)^{+\bullet}$ cation radicals could not be studied because the formation of the $(TTT+2H)^{2+}$ precursor dications was prevented by the low basicity of thymine.[48]

Major differences, depending on the type of the nucleobase, were observed for backbone dissociations where the mass identity of the $\boldsymbol{w}_2^{+}$ and $\boldsymbol{d}_2^{+}$ fragment ions was resolved by ^{15}N labeling (Figures S10−S12 in the Supporting Information). Backbone cleavage in $(AAA+2H)^{+\bullet}$ was nonspecific, showing a 55:45 ratio for the formation of the $\boldsymbol{w}_2^{+}$ and $\boldsymbol{d}_2^{+}$ fragment ions that both appeared at m/z 645 in the Figure 4a spectrum but were resolved by ^{15}N labeling (Figure S10). These were both even-electron ions, indicating that they were formed by elimination of neutral radicals. In contrast to $(AAA+2H)^{+\bullet}$, the backbone dissociations of $(CCC+2H)^{+\bullet}$ unequivocally formed even-electron $\boldsymbol{d}_2^{+}$ ions at m/z 597 (Figure 4b). This can be realized by one-step elimination of the complementary $\boldsymbol{z}_1^{\bullet}$ radicals from $(CCC+2H)^{+\bullet}$ or by consecutive loss of 3′-cytosine, followed by elimination of a $C_5H_7O_2$ radical from the 3′-deoxyribose residue. The favored loss of 3′-cytosine (Figure S11) appeared to be consistent with the latter two-step mechanism. The spectrum also showed hydrogen migrations resulting in the formation of $(\boldsymbol{d}_2+H)^{+\bullet}$ and $(\boldsymbol{d}_2+2H)^{+}$ ions at m/z 598 and 599, respectively (Figure 4b). The $\boldsymbol{d}_2^{+}$ and $(\boldsymbol{d}_2+2H)^{+}$ ions were identified by ^{15}N-labeling (Figure S11 in the Supporting Information), which showed that the isomeric $\boldsymbol{w}_2^{+}$ ions were absent. A specific feature of cation radicals containing 5′-cytosine was a direct elimination of water, as also observed for other codons of the $(CXY+2H)^{+\bullet}$ type. A still different pattern was found for the CID-MS^3 spectra of $(GGG+2H)^{+\bullet}$, which showed odd-electron $(\boldsymbol{w}_2+H)^{+\bullet}$ fragment ions (m/z 678) that were accompanied by their even-electron $\boldsymbol{w}_2^{+}$ counterparts at m/z 677 (Figure 4c). The spectra of the ^{15}N-analogues (Figure S12) confirmed that the formation of the $\boldsymbol{d}_2^{+}$ ions from $(GGG+2H)^{+\bullet}$, to be expected at m/z 683 from the 5′-labeled GGG, was negligibly small. The formation of the $(\boldsymbol{w}_2+H)^{+\bullet}$ ions indicated retention of the added hydrogen atom in one of the remaining middle or 3′-guanine residues, which raised the question of the proton and hydrogen atom sites in the $(GGG+2H)^{+\bullet}$ ions and their possible migrations in the course of dissociation.

Overall, the differences in the dissociations of the $(AAA+2H)^{+\bullet}$, $(CCC+2H)^{+\bullet}$, and $(GGG+2H)^{+\bullet}$ cation radicals were quite remarkable, especially in comparison to backbone dissociations of their closed-shell mono- and dication analogues,[47,48] which unambiguously formed $\boldsymbol{w}_2^{+}$ backbone ions from most sequences. This pointed out the role of the radical sites in the cation radicals and their effect on steering the dissociations.

Resolution of Identity in Dissociations of Codons of the $(XYX+2H)^{+\bullet}$ Type. Having resolved the dissociations of base-homologous codon cation radicals, we systematically replaced one or more nucleobases to investigate the effect of the distinct base on the dissociations. Starting with the replacement of the middle base, the codon table provides 12 XYX combinations of the centrosymmetric type, for which we were able to generate a complete set of cation radicals and obtain their CID-MS^3 spectra. Mass identity in dissociations due to the 5′- and 3′-nucleobases was resolved by ^{15}N labeling in the 5′-nucleobase. The spectra of $(ACA+2H)^{+\bullet}$ (Figure S9a,b), $(AGA+2H)^{+\bullet}$ (Figure S2b,c), and $(ATA+2H)^{+\bullet}$ (Figure S2e,f) showed a nonspecific loss of 5′- and 3′-adenine that was accompanied by the formation of the $\boldsymbol{w}_2^{+}$ and $\boldsymbol{d}_2^{+}$ backbone fragment ions. These were resolved by ^{15}N labeling, showing a slight preference for the $\boldsymbol{d}_2^{+}$ ion formation (Figure S2). The spectra also showed prominent $\boldsymbol{w}_1^{+}$ ions at m/z 332 which, however, were not accompanied by abundant $\boldsymbol{d}_1^{+}$ counterparts.

The spectra of $(CAC+2H)^{+\bullet}$, $(CGC+2H)^{+\bullet}$ (Figure S1e,f), and $(CTC+2H)^{+\bullet}$ (Figure S3b) were qualitatively similar to that of $(CCC+2H)^{+\bullet}$, as evidenced by the facile formation od $\boldsymbol{d}_2^{+}$ backbone ions. However, the patterns for the loss of nucleobase substantially differed, depending on the middle nucleobase. For $(CAC+2H)^{+\bullet}$, we observed no fragment ions by loss of cytosine and very minor loss of adenine from the precursor cation radical. In contrast, loss of cytosine proceeded abundantly from the $\boldsymbol{d}_2^{+}$ ion (m/z 621) to produce the m/z 510 secondary ion. The spectrum of the $(CGC+2H)^{+\bullet}$ ion showed an unusual loss of guanine radical ($G^{\bullet}$, 150 Da, m/z 697) while the loss of cytosine was accompanied by an elimination of 44 and 57 Da neutral fragments, most likely C_2H_4O and $C_3H_5O^{\bullet}$, respectively, from cross-ring cleavage of the deoxyribose radical. The spectrum of the $(CTC+2H)^{+\bullet}$ ion (Figure S3b) showed a dominant loss of cytosine and also loss of a thymine radical ($T^{\bullet}$, 125 Da, m/z 697). These were all radical reactions that had no equivalents in closed-shell ion dissociations. The backbone cleavage yielding the $\boldsymbol{d}_2$ ion at m/z 612 was accompanied by hydrogen transfer forming the less usual $(\boldsymbol{d}_2-H)^{+\bullet}$ cation radical at m/z 611. Noteworthy was the direct loss of water from $(CTC+2H)^{+\bullet}$ (Figure S3b).

The spectra of $(GAG+2H)^{+\bullet}$, $(GCG+2H)^{+\bullet}$, and $(GTG+2H)^{+\bullet}$ (Figure S8d−f) showed the predominant loss of guanine that occurred chiefly from the 5′-position, as resolved by ^{15}N-labeling. The backbone dissociations involved hydrogen transfers to yield $(\boldsymbol{w}_2+H)^{+\bullet}$ fragment ions that were accompanied by the more common $\boldsymbol{w}_2^{+}$ ions. This pattern was similar to that observed for $(GGG+2H)^{+\bullet}$ and appeared to be driven by the loss of 5′-guanine. The dissociations of $(GCG+2H)^{+\bullet}$ were outstanding in that they resulted in the formation of even-electron $(\boldsymbol{d}_2+2H)^{+}$ ions (m/z 644) that must have involved a double hydrogen atom transfer from the complementary $\boldsymbol{z}_1$ fragment.

The spectra of $(TAT+2H)^{+\bullet}$, $(TCT+2H)^{+\bullet}$, and $(TGT+2H)^{+\bullet}$ (Figures S9h,i and S6f) showed a great diversity in the types of dissociations, strongly depending on the central nucleobase. This effect was understandable, because the central nucleobase was substantially more basic than thymine and was likely to retain the charging proton. Unfortunately, double protonation of these trinucleotides was very inefficient due to the low basicity of thymine and did not allow us to obtain spectra of the ^{15}N-labeled derivatives. For this reason, the fragment ion assignment is only tentative. The spectrum of $(TAT+2H)^{+\bullet}$ (Figure S9h) showed a major fragment by loss of water (m/z 843) and an unusual ion at m/z 820. This could logically result by elimination of C_2HO by ring cleavage in one of the thymines. Backbone cleavage was observed as $\boldsymbol{w}_2^{+}/\boldsymbol{d}_2^{+}$ and $(\boldsymbol{w}_2+2H)^{+}/(\boldsymbol{d}_2+2H)^{+}$ even-electron fragment ions. The spectrum of $(TGT+2H)^{+\bullet}$ (Figure S6f) displayed a major fragment ion by loss of water (m/z 859) and a cluster of $\boldsymbol{w}_2^{+}/\boldsymbol{d}_2^{+}$ ions at m/z 652 including their hydrogen-transfer analogues at adjacent m/z values. Deoxyribose cross-ring fragments were present at m/z 707 and 694 that presumably were formed by loss of C_2H_4O and $C_3H_5O^{\bullet}$, respectively,

https://doi.org/10.1021/jasms.2c00322
J. Am. Soc. Mass Spectrom. 2023, 34, 304−319

Scheme 5. Calculated Structures and Relative Energies for d_2^+ Ion Formation from $(CCC+2H)^{+\bullet}$[a]

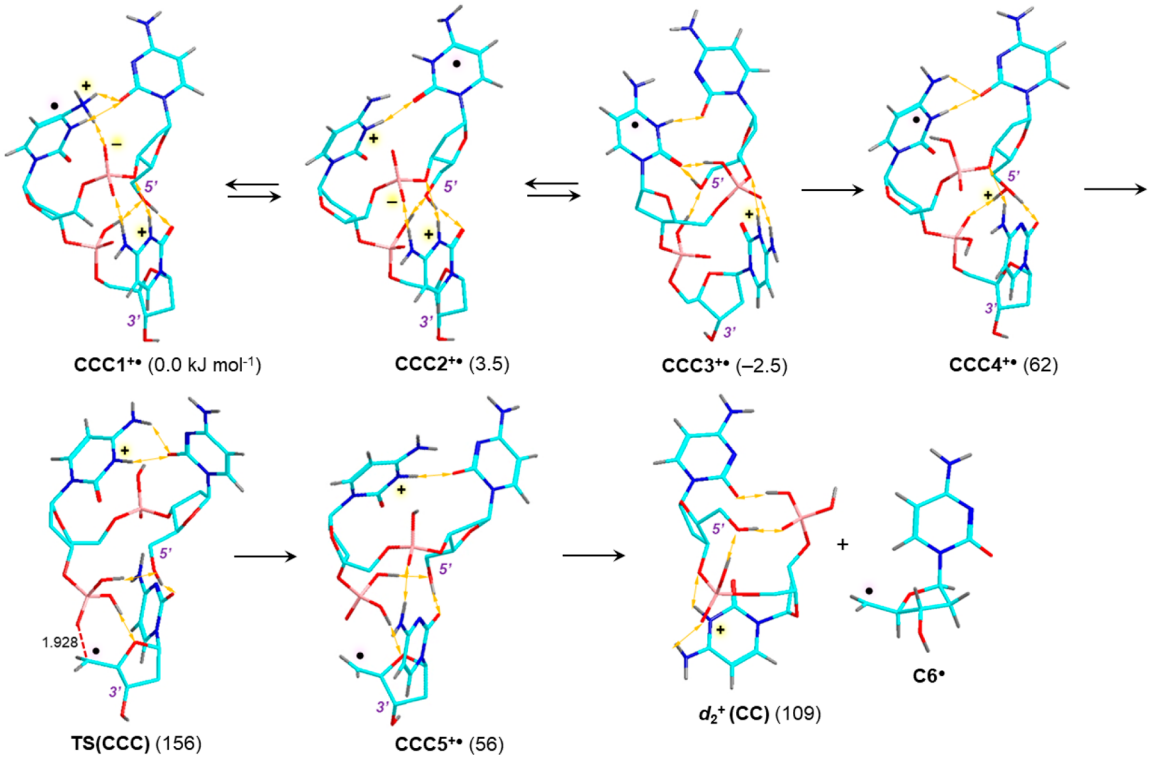

[a]Atom color coding is as follows: cyan, C; red, O; blue, N; gray, H; bronze, P. Only nucleobase and exchangeable hydrogen atoms are shown to avoid clutter. Relative energies are from M06-2X/6-311++G(2d,p) single-point calculations including zero-point vibrational corrections and referenced to 0 K. Radical locations were assigned from atomic spin densities calculated by a natural population analysis of the M06-2X/6-311++G(2d,p) wave functions.

Scheme 6. Higher-Energy Pathway to the d_2^+ Ion Formation from $(CCC+2H)^{+\bullet}$ [a]

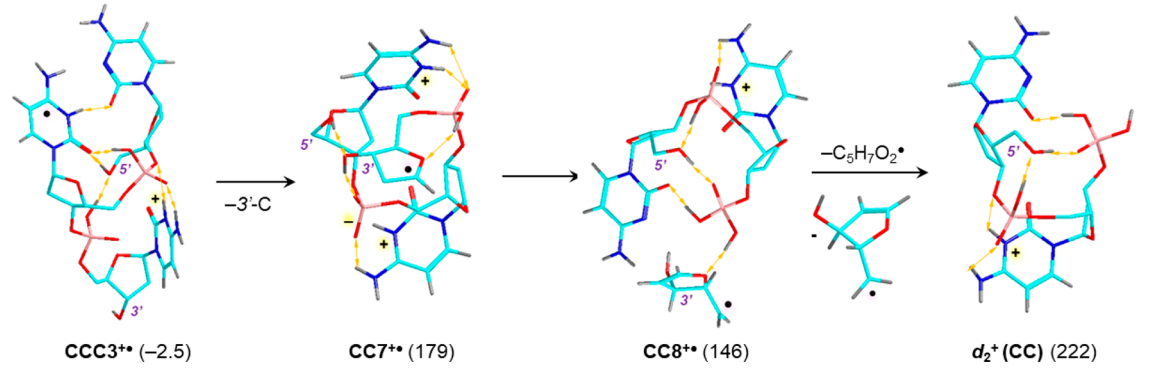

[a]Description as in Scheme 5.

following the loss of thymine (m/z 751). It may be noted that protonation of thymine in trinucleotides has been found to be energetically disfavored, as judged by $(TTT+H)^+$, in which low-energy structures were protonated at the phosphate ester groups instead in thymine.[48] This is expected to have a large effect on the structures of the $(TXT+2H)^{2+}$ precursor dications and $(TXT+2H)^{+\bullet}$ cation radicals.

Ion Structures and Energetics. $(CCC+2H)^{+\bullet}$ was the typical representative of the ion group undergoing backbone dissociations to form d_2^+ ions. From combined BOMD trajectory and DFT gradient optimization calculations of all theoretically possible protomers carrying protons at cytosine positions N3 and O2, we obtained equilibrium geometries of several isomers; the lowest Gibbs-energy structures **CCC1**$^{+\bullet}$–**CCC3**$^{+\bullet}$ are shown in Scheme 5. These nearly isoenergetic $(CCC+2H)^{+\bullet}$ ions substantially differed in their electronic structure. **CCC1**$^{+\bullet}$ was a zwitterion with a negative phosphate group between the 5′- and middle nucleosides. The 3′-base was protonated at N3, whereas the middle base carried a proton and a hydrogen atom that showed tight hydrogen bonds to the 5′-cytosine O2 and the phosphate anion. **CCC2**$^{+\bullet}$ was another zwitterion with the middle and 3′-bases protonated and the 5′-base carrying the hydrogen atom. **CCC3**$^{+\bullet}$ was a canonical structure in which the 3′-base was protonated and the middle base was a radical. The nearly isoenergetic nature of these structures, as well as their formation by electron and proton migrations upon BOMD, indicated that these isomerizations were facile, in part due to

https://doi.org/10.1021/jasms.2c00322
J. Am. Soc. Mass Spectrom. 2023, 34, 304−319

Scheme 7. Calculated Structures and Relative Energies of $(GGG+2H)^{+\bullet}$ [a]

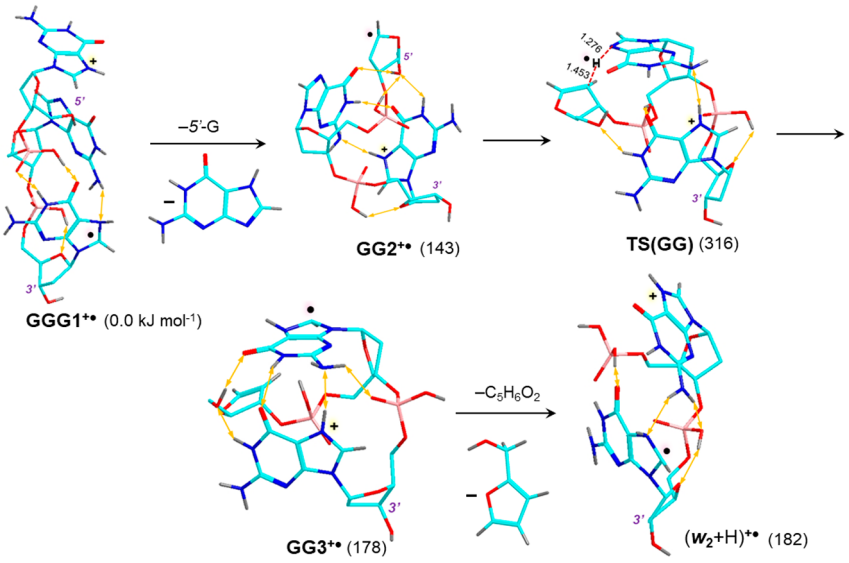

[a]Description as in Scheme 5.

the interconnecting hydrogen bonds with the phosphate groups that relayed protons within the ions. The lowest energy pathway we found for the dissociation and formation of the d_2^+ ion is shown in Scheme 5. This involved proton migration onto the lower phosphate ester group, where it was shared by a strong hydrogen bond with the 5′-hydroxyl. This intermediate (**CCC4**$^{+\bullet}$) was a local energy minimum at 62 kJ mol^{-1} relative to **CCC1**$^{+\bullet}$. Homolytic cleavage of the O5−C5′ bond was associated with proton and electron migration to reach **TS(CCC)** at 156 kJ mol^{-1} relative to **CCC1**$^{+\bullet}$, representing an unusually low energy barrier. Interestingly, the dissociation was accompanied by electron transfer and spin density migration from the middle cytosine in **CCC4**$^{+\bullet}$ to the 3′-deoxyribose methylene group in **TS(CCC)** (Scheme 5). The dissociation further proceeded to a complex of the incipient z_1 radical **C6**$^{\bullet}$ and d_2^+ (CC) ion that upon separating to the products achieved the 109 kJ mol^{-1} thermochemical threshold. We did not include in the product energy calculations corrections to the basis set superposition error that could further lower the threshold energy by a few kJ mol^{-1}. The low energy threshold and TS energy were consistent with the very facile formation of the d_2^+ ions from $(CCC+2H)^{+\bullet}$. We presume that an analogous mechanism can be applied to the formation of d_2^+ ions from the other trinucleotide cation radicals having 3′-cytosine.

The alternative pathway *a*, shown generically in Scheme 1, was calculated to be substantially less favorable (Scheme 6). Loss of the 3′-cytosine required 179 kJ mol^{-1} to form the zwitterionic intermediate **CC7**$^{+\bullet}$, which already was above the energy of **TS(CCC)** in pathway *b*. Homolytic cleavage of the O5−C5′ bond in **CC7**$^{+\bullet}$ led to a complex (**CC8**$^{+\bullet}$) at 146 kJ mol^{-1} relative to **CCC1**$^{+\bullet}$, and further fragment separation required additional 76 kJ mol^{-1}, placing the thermochemical threshold at 222 kJ mol^{-1} relative to **CCC1**$^{+\bullet}$.

To elucidate the formation of $(w_2+H)^{+\bullet}$ ions, we obtained optimized structures of low-energy $(GGG+2H)^{+\bullet}$ ions (Scheme 7). The calculations unequivocally pointed to structure **GGG1**$^{+\bullet}$ as the lowest-energy protomer in which the 5′-guanine was protonated at the most basic N7 position while the 3′-guanine carried the hydrogen radical. There were no zwitterionic isomers among the low-energy $(GGG+2H)^{+\bullet}$ structures. This was consistent with a previous computational study of $(GGG+H)^+$ ions that also found no low-energy zwitterions.[48] Loss of 5′-guanine as a less stable N7−H tautomer was calculated to have a thermochemical threshold at 143 kJ mol^{-1}, forming the ion **GG2**$^{+\bullet}$ as the lowest energy structure, which was a 5′-deoxyribose radical. The correlation of the ion electronic structures in the **GGG1**$^{+\bullet}$ → **GG2**$^{+\bullet}$ reaction step indicated that the reaction must be accompanied by electron transfer from the 3′-guanine radical to 5′-deoxyribose. The timing of this electron transfer was not studied; it may occur in a low-lying excited electronic state of **GGG1**$^{+\bullet}$, which we calculated to be 2.60 eV (251 kJ mol^{-1}) above the ground state and could be accessed by collisional excitation within the internal energy range needed for the dissociation (316 kJ mol^{-1}, Scheme 7). Alternatively, loss of 5′-guanine may initially proceed via an ionic mechanism by heterolysis of the C1′−N7 bond, and the product or intermediates can undergo electron transfer to reach the lowest energy structure **GG2**$^{+\bullet}$. In the next step, hydrogen transfer to the middle guanine required 316 kJ mol^{-1} in **TS(GG)** to produce an intermediate (**GG3**$^{+\bullet}$) at 178 kJ mol^{-1} relative to **GGG1**$^{+\bullet}$. Loss of furfuryl alcohol by phosphate ester elimination in **GG3**$^{+\bullet}$ was only 4 kJ mol^{-1} endergonic forming the $(w_2+H)^{+\bullet}$ ion, although this dissociation may involve an energy barrier. Overall, the pathway described in Scheme 7 was compatible with the identity-resolved CID-MS^3 spectrum of $(GGG+2H)^{+\bullet}$. The spectrum showed abundant fragment ions by loss of 5′-guanine, which was conducive to the formation of the $(w_2+H)^{+\bullet}$ ion. Conversely, the $(w_2+H)^{+\bullet}$ relative intensity in the spectrum was relatively low, which was consistent with the calculated high activation energy for **TS(GG)** in the hydrogen migration step, kinetically stabilizing the **GG2**$^{+\bullet}$ intermediate.

We suggest that the Scheme 7 mechanism, considering an initial loss of the 5′-base, can be applied to explain dissociations of most trinucleotide cation radicals of the $(w_2+H)^{+\bullet}$ group. Figures S7 and S8 in the Supporting Information document that most of the ions in this group have 5′-guanine, whose loss initiates the subsequent hydrogen

https://doi.org/10.1021/jasms.2c00322
J. Am. Soc. Mass Spectrom. 2023, 34, 304−319

Scheme 8. Calculated Structures and Relative Energies for the Competitive Formation of w_2^+ and d_2^+ Ions from $(AAA+2H)^{+\bullet}$ [a]

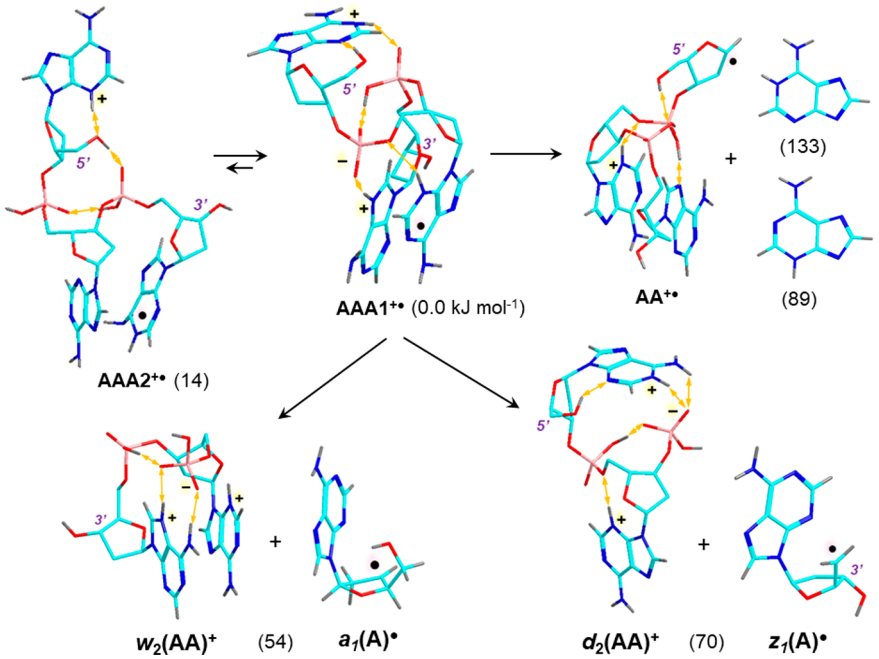

[a]Description as in Scheme 5.

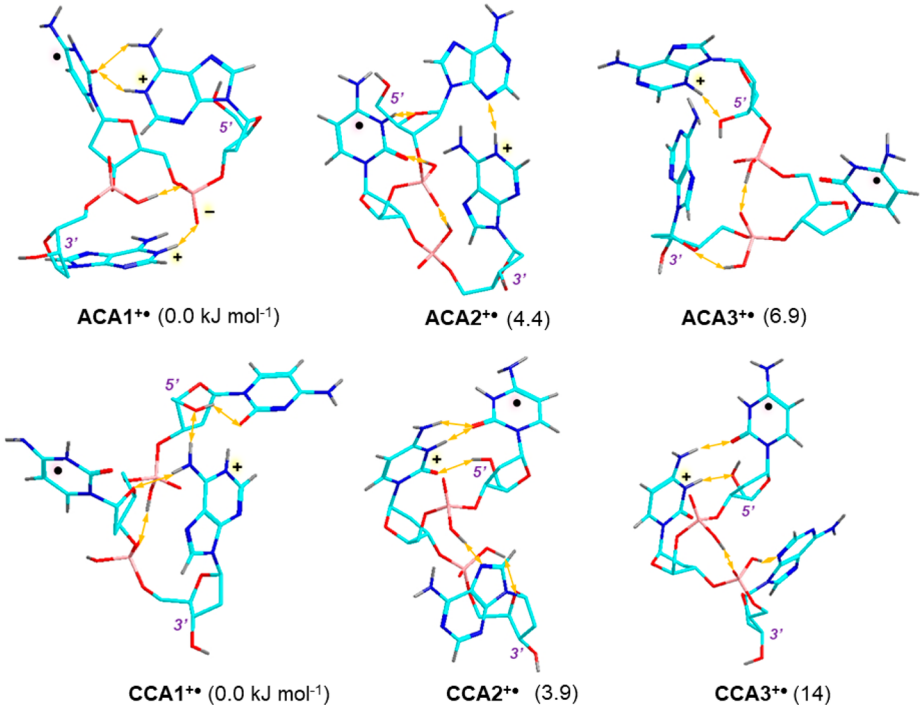

Figure 5. Calculated structures of low-energy $(ACA+2H)^{+\bullet}$ and $(CCA+2H)^{+\bullet}$ ions. Structure description as in Scheme 5.

transfer and elimination of $C_5H_6O_2$. Formation of $(w_2+H)^{+\bullet}$ ions was also observed for trinucleotide cation radicals having a 5′-adenine, such as $(AAG+2H)^{+\bullet}$ (Figure S7a), $(AGG+2H)^{+\bullet}$, and $(ATG+2H)^{+\bullet}$ (Figure S8a,b), although in these cases it competed with other backbone cleavages: namely, those forming w_2^+ and d_2^+ ions. It may be argued that protonation at 5′-adenine and guanine can occur competitively with these sequences to provide intermediates for the 5′-adenine loss, which was observed as an abundant dissociation in the spectra. The formation of $(w_2+H)^{+\bullet}$ ions from $(CGG+2H)^{+\bullet}$ (Figure S8c) was in fact a less abundant process that occurred in competition with dissociations yielding $(w_2-H)^{+\bullet}$ and w_2^+ ions. Prominent formation of $(w_2-H)^{+\bullet}$ ions was also observed for $(CCG+2H)^{+\bullet}$ (Figure S9g), indicating a reverse hydrogen transfer to the departing 5′-cytosine.

Dissociations of the $(AAA+2H)^{+\bullet}$ ions revealed competitive formation of w_2^+ and d_2^+ ions, as resolved by ^{15}N-labeling (Figure S10). Using BOMD and DFT calculations, we

https://doi.org/10.1021/jasms.2c00322
J. Am. Soc. Mass Spectrom. 2023, 34, 304−319

obtained optimized structures of the relevant species. (AAA +2H)$^{+\bullet}$ ions were found to prefer zwitterionic structures that were produced by one-electron reduction of low-energy zwitterionic dications.[48] This is illustrated with **AAA1**$^{+\bullet}$ (Scheme 8) that was a zwitterion protonated at 5′-N1 and 3′-N7 whereas the radical was in the middle adenine base. The nearest-energy canonical structure (**AAA2**$^{+\bullet}$) was protonated at 5′-N3 with the radical being in the 3′-base. Loss of 5′-adenine from **AAA1**$^{+\bullet}$ should lead to ion **AA**$^{+\bullet}$ as the lowest-energy protomer having the radical at 5′-C1′. Although the structure **AAA1**$^{+\bullet}$ correlates with the less stable adenine N1−H tautomer, proton transfer between the 5′-adenine and the proximate phosphate group could deliver the proton to N3, as it is in **AAA2**$^{+\bullet}$, and produce the lower energy N3−H adenine tautomer. The calculated dissociation energy for the latter was rather low at 89 kJ mol^{-1}, which was consistent with the facile adenine loss. Remarkably, the formation of the lowest-energy cation radical **AA**$^{+\bullet}$ necessitated electron transfer from the adenine radical to the C1′ position at 5′-deoxyribose. The competitive formations of the w_2^+ and d_2^+ ions were calculated to both have low and very similar threshold energies. The branching ratio for these two dissociations obviously depends on the kinetics in the relevant rate-determining steps. Nevertheless, the calculated threshold energies, favoring the formation of w_2^+ and $a_1^\bullet$, were consistent with the w_2^+ and d_2^+ fragment ion distribution in the CID-MS^3 spectrum (Figure S10).

Dissociations forming the $(d_2+2H)^+$ ions were prominently represented with sequences having a middle-cytosine-3′-purine arrangement, such as in (ACA+2H)$^{+\bullet}$, (ACG+2H)$^{+\bullet}$, (TCA +2H)$^{+\bullet}$, (GCA+2H)$^{+\bullet}$, (CCA+2H)$^{+\bullet}$, and (CCG+2H)$^{+\bullet}$ (Figure S9a−g). To elucidate the electronic effects leading to this unusual dissociation, we addressed by combined BOMD and DFT calculations the structures of (ACA+2H)$^{+\bullet}$ and (CCA+2H)$^{+\bullet}$ (Figure 5). The three lowest-energy (ACA +2H)$^{+\bullet}$ ions, **ACA1**$^{+\bullet}$, **ACA2**$^{+\bullet}$, and **ACA3**$^{+\bullet}$, were nearly isoenergetic according to M06-2X calculations. All three structures had the radical delocalized between C4 and C6 in the cytosine base, while the proton distribution patterns differed.

ACA1$^{+\bullet}$ was a zwitterion in which 3′- and 5′-adenine were protonated at N1, and the overall charge balance was maintained by the phosphate anion between the middle and 5′-nucleoside. **ACA2**$^{+\bullet}$ and **ACA3**$^{+\bullet}$ were canonical cation-radical structures that were protonated at N1-3′- and N3-5′-adenine, respectively. The very similar relative energies of these protomers, as well as their multiple hydrogen bonds connecting the backbone phosphates and nucleobases, indicated that the cation radicals could undergo facile interconversions. The low-energy (CCA+2H)$^{+\bullet}$ ions were all canonical cation radicals. The nearly isoenergetic **CCA1**$^{+\bullet}$ and **CCA2**$^{+\bullet}$ differed in the position of the radical, which was at the middle cytosine in the former and at 5′-cytosine in the latter. Ion **CCA3**$^{+\bullet}$ was a higher-energy conformer of **CCA2**$^{+\bullet}$, from which it differed by the orientation of 3′-adenosine. The common feature of the (ACA+2H)$^{+\bullet}$ and (CCA+2H)$^{+\bullet}$ ions was the presence of a cytosine radical in the middle position or its facile formation by hydrogen transfer. This indicated that the cytosine radical played a role in hydrogen transfer from the 3′-nucleoside to trigger dissociation leading to $(d_2+2H)^+$ ions. We examined the hydrogen transfer energetics with model cytidine radicals (Scheme S1 in the Supporting Information). Transfer to cytosine C6 of deoxyribose H1′ or H3′ was 73 kJ mol^{-1} endergonic, which was well within the range of dissociation energies for trinucleotide cation radicals (*vide supra*). The energetics for the 3′-deoxyribose hydrogen migrations onto C6 in the middle cytosine radical in **CCA2**$^{+\bullet}$ was similar to that in the model cytidines, 92 and 87 kJ mol^{-1} for H1′ and H4′, in the respective intermediates **CCA4**$^{+\bullet}$ and **CCA5**$^{+\bullet}$ (Scheme S2 in the Supporting Information). While these energies were within the range of those for other trinucleotide cation radical dissociations, they allowed for competition with the loss of $CH_2OH^\bullet$ from the 5′-sugar and backbone dissociation to w_2^+ ions from (CCA +2H)$^{+\bullet}$ (Figure S9f) that are likely to be radical-initiated. The loss of $CH_2OH^\bullet$ could originate from the low-energy structure **CCA2**$^{+\bullet}$ that had a sterically favorable arrangement of the 5′-cytosine radical and deoxyribose. Similarly, the formation of the w_2^+ ion can be initiated by 5′-cytosine loss in **CCA2**$^{+\bullet}$. Returning back to $(d_2+2H)^+$ ions, the formation of the 3′-sugar radicals in **CCA4**$^{+\bullet}$ and **CCA5**$^{+\bullet}$ was expected to weaken the PO−C5′ bond in 3′-deoxyribose to facilitate elimination of the (z_1-H) radical and formation of the $(d_2+2H)^+$ ion.

CONCLUSIONS

CID-MS^3 spectra of 60 trinucleotide cation radicals, reported here, displayed a variety of dissociations that were triggered by radicals residing in the nucleobases. The radical sites were created by electron attachment to a protonated nucleobase or after hydrogen atom transfer to a neutral nucleobase, which were primarily cytosine or thymine of high hydrogen atom affinities. Dissociations forming standard d_2^+ and w_2^+ backbone fragments were promoted by hydrogen atom radical migrations that substantially lowered the threshold energies. In addition, multiple hydrogen atom migrations accompanied the backbone dissociations, resulting in the formation of novel $(w_2+H)^{+\bullet}$, $(w_2+2H)^+$, and $(d_2+2H)^+$ fragment ions. These dissociations were linked to the presence and sequence position of particular nucleobases. Guanine residues supported dissociations producing $(w_2+H)^{+\bullet}$ ions. Cytosine and thymine nucleobases in 3′- and 5′-positions triggered cross-ring cleavages and loss of CH_2OH, respectively, in the terminal deoxyriboses. DFT calculations of trinucleotide cation radical structures and energies led us to conclude that adenine-rich trinucleotide cation radicals in the AAA and ACA combinations existed as low-energy zwitterionic structures. In contrast, guanine nucleotides did not favor zwitterionic structures. The calculations also indicated very low threshold energies for the radical dissociations, which was consistent with the rich chemistry of these cation radicals.

ASSOCIATED CONTENT

Supporting Information

The Supporting Information is available free of charge at https://pubs.acs.org/doi/10.1021/jasms.2c00322.

Supplementary CID-MS^3 spectra and optimized structures (PDF)

AUTHOR INFORMATION

Corresponding Authors

František Tureček − *Department of Chemistry, Bagley Hall, Box 351700, University of Washington, Seattle, Washington 98195-1700, United States;* orcid.org/0000-0001-7321-7858; Phone: +1-206-685-2041l; Email: turecek@uw.edu

https://doi.org/10.1021/jasms.2c00322
J. Am. Soc. Mass Spectrom. 2023, 34, 304−319

Aleš Marek − *Institute of Organic Chemistry and Biochemistry, Czech Academy of Sciences, 16610 Prague 6, Czech Republic;* orcid.org/0000-0001-9031-8263; Email: ales.marek@uochb.cas.cz

Authors

Jiahao Wan − *Department of Chemistry, Bagley Hall, Box 351700, University of Washington, Seattle, Washington 98195-1700, United States*

Břetislav Brož − *Institute of Organic Chemistry and Biochemistry, Czech Academy of Sciences, 16610 Prague 6, Czech Republic;* orcid.org/0000-0002-2142-1045

Yue Liu − *Department of Chemistry, Bagley Hall, Box 351700, University of Washington, Seattle, Washington 98195-1700, United States*

Shu R. Huang − *Department of Chemistry, Bagley Hall, Box 351700, University of Washington, Seattle, Washington 98195-1700, United States*

Complete contact information is available at: https://pubs.acs.org/10.1021/jasms.2c00322

Notes

The authors declare no competing financial interest.

■ ACKNOWLEDGMENTS

Research at the University of Washington was supported by the Chemistry Division of the U.S. National Science Foundation, Grant CHE-1951518. F.T. acknowledges support by the Klaus and Mary Ann Saegebarth Endowment. Research at the IOCB was supported by the Ministry of Education, Youth and Sport (MSMT INTER-EXCELLENCE LTAUSA19094).

■ REFERENCES

(1) Ward, J. Complexity of Damage Produced by Ionizing Radiation; in *Cold Spring Harbor Symposia on Quantitative Biology*; Cold Spring Harbor Laboratory Press: 2000; pp 377−382.

(2) von Sonntag, C. *Free-Radical-Induced DNA Damage and Its Repair*; Springer: 2006.

(3) Sanche, L. Low Energy Electron-Driven Damage in Biomolecules. *Eur. Phys. J. D Atomic, Molecular, Optical and Plasma Physics* **2005**, *35*, 367−390.

(4) Alizadeh, E.; Orlando, T. M.; Sanche, L. Biomolecular Damage Induced by Ionizing Radiation: the Direct and Indirect Effects of Low-Energy Electrons on DNA. *Annu. Rev. Phys. Chem.* **2015**, *66*, 379−398.

(5) Giese, B. Long-Distance Charge Transport in DNA: The Hopping Mechanism. *Acc. Chem. Res.* **2000**, *33*, 631−636.

(6) Giese, B. Long-Distance Electron Transfer Through DNA. *Annu. Rev. Biochem.* **2002**, *71*, 51−70.

(7) Douki, T.; Ravanat, J.-L.; Angelov, D.; Wagner, J. R.; Cadet, J. Effects of Duplex Stability on Charge-Transfer Efficiency within DNA. *Top. Curr. Chem.* **2004**, *236*, 1−25.

(8) Takada, T.; Kawai, K.; Fujitsuka, M.; Majima, T. Direct Observation of Hole Transfer through Double-Helical DNA over 100 A. *Proc. Natl. Acad. Sci. U. S. A.* **2004**, *101*, 14002−14006.

(9) *Charge Transfer in DNA*; Wagenknecht, H.-A., Ed.; Wiley-VCH: 2005.

(10) Gray, H. B. *Charge Transfer in DNA: from Mechanism to Application*; Wiley: 2006.

(11) Genereux, J. C.; Boal, A. K.; Barton, J. K. DNA-Mediated Charge Transport in Redox Sensing and Signaling. *J. Am. Chem. Soc.* **2010**, *132*, 891−905.

(12) Kawai, K.; Majima, T. Hole Transfer Kinetics of DNA. *Acc. Chem. Res.* **2013**, *46*, 2616−2625.

(13) Adhikary, A.; Collins, S.; Khanduri, D.; Sevilla, M. D. Sugar Radicals Formed by Photoexcitation of Guanine Cation Radical in Oligonucleotides. *J. Phys. Chem. B* **2007**, *111*, 7415−7421.

(14) Chen, H.-Y.; Kao, C.-L.; Hsu, S. C. N. Proton Transfer in Guanine-Cytosine Radical Anion Embedded in B-Form DNA. *J. Am. Chem. Soc.* **2009**, *131*, 15930−15938.

(15) Choi, J.; Yang, C.; Fujitsuka, M.; Tojo, S.; Ihee, H.; Majima, T. Proton Transfer of Guanine Radical Cations Studied by Time-Resolved Resonance Raman Spectroscopy Combined with Pulse Radiolysis. *J. Phys. Chem. Lett.* **2015**, *6*, 5045−5050.

(16) Rodriguez-Santiago, L.; Noguera, M.; Bertan, J.; Sodupe, M. Hydrogen Bonding and Proton Transfer in Ionized DNA Base Pairs, Amino Acids and Peptides. In *Quantum Biochemistry*; Matt, C. F., Ed.; Wiley-VCH: 2010; pp 219−242.

(17) Joy, A.; Ghosh, A. K.; Schuster, G. B. One-Electron Oxidation of DNA Oligomers That Lack Guanine: Reaction and Strand Cleavage at Remote Thymines by Long-Distance Radical Cation Hopping. *J. Am. Chem. Soc.* **2006**, *128*, 5346−5347.

(18) Ghosh, A.; Joy, A.; Schuster, G. B.; Douki, T.; Cadet, J. Selective One-Electron Oxidation of Duplex DNA Oligomers: Reaction at Thymines. *Org. Biomol. Chem.* **2008**, *6*, 916−928.

(19) Joseph, J.; Schuster, G. B. Oxidatively Damaged Nucleobases in Duplex DNA Oligomers: Reaction at Thymine-Thymine Mispairs. *J. Am. Chem. Soc.* **2009**, *131*, 13904−13905.

(20) Kanvah, S.; Schuster, G. B. One-Electron Oxidation of DNA: Thymine versus Guanine Reactivity. *Org. Biomol. Chem.* **2010**, *8*, 1340−1343.

(21) Barnett, R. N.; Joseph, J.; Landman, U.; Schuster, G. B. Oxidative Thymine Mutation in DNA: Water-Wire-Mediated Proton-Coupled Electron Transfer. *J. Am. Chem. Soc.* **2013**, *135*, 3904−3914.

(22) Boudaıffa, B.; Cloutier, P.; Hunting, D.; Huels, M. A.; Sanche, L. Resonant Formation of DNA Strand Breaks by Low-Energy (3 to 20 eV) Electrons. *Science* **2000**, *287* (5458), 1658−1660.

(23) Wang, C.-R.; Nguyen, J.; Lu, Q.-B. Bond Breaks of Nucleotides by Dissociative Electron Transfer of Nonequilibrium Prehydrated Electrons: A New Molecular Mechanism for Reductive DNA Damage. *J. Am. Chem. Soc.* **2009**, *131*, 11320−11322.

(24) Steenken, S. Purine Bases, Nucleosides, and Nucleotides: Aqueous Solution Redox Chemistry and Transformation Reactions of Their Radical Cations and e- and OH Adducts. *Chem. Rev.* **1989**, *89*, 503−520.

(25) Candeias, L. P.; Steenken, S. Electron Adducts of Adenine Nucleosides and Nucleotides in Aqueous Solution: Protonation at Two Carbon Sites (C2 and C8) and Intra- and Intermolecular Catalysis by Phosphate. *J. Phys. Chem. A* **1992**, *96*, 937−944.

(26) Candeias, L. P.; Wolf, P.; O'Neill, P.; Steenken, S. Reaction of Hydrated Electrons with Guanine Nucleosides: Fast Protonation on Carbon of the Electron Adduct. *J. Phys. Chem. A* **1992**, *96*, 10302−10307.

(27) Barnes, J.; Bernhard, W. A. The Protonation State of One-Electron Reduced Cytosine and Adenine. 1. Initial Protonation Sites at Low Temperatures in Glassy Solids. *J. Phys. Chem. A* **1993**, *97*, 3401−3408.

(28) Barnes, J.; Bernhard, W. A. One-Electron-Reduced Cytosine in Acidic Glasses: Conformational States before and after Proton Transfer. *J. Phys. Chem. A* **1994**, *98*, 10969−10977.

(29) Steenken, S.; Jovanovic, S. V. How Easily Oxidizable Is DNA? One-Electron Reduction Potentials of Adenosine and Guanosine Radicals in Aqueous Solution. *J. Am. Chem. Soc.* **1997**, *119*, 617−618.

(30) Wolken, J. K.; Syrstad, E. A.; Vivekananda, S.; Tureček, F. Uracil Radicals in the Gas Phase. Specific Generation and Energetics. *J. Am. Chem. Soc.* **2001**, *123*, 5804−5805.

(31) Syrstad, E. A.; Vivekananda, S.; Tureček, F. Direct Observation of a Hydrogen Atom Adduct to C-5 in Uracil. A Neutralization-Reionization Mass Spectrometric and ab initio Study. *J. Phys. Chem. A* **2001**, *105*, 8339−8351.

(32) Wolken, J. K.; Tureček, F. Direct Observation of a Hydrogen Atom Adduct to O-4 in Uracil. A Neutralization-Reionization Mass

Spectrometric and Ab initio Study. *J. Phys. Chem. A* **2001**, *105*, 8352−8360.
(33) Chen, X.; Syrstad, E. A.; Nguyen, M. T.; Gerbaux, P.; Tureček, F. Adenine Radicals in the Gas Phase. An Experimental and Computational Study of Hydrogen Atom Adducts to Adenine. *J. Phys. Chem. A* **2005**, *109*, 8121−8132.
(34) Yao, C.; Cuadrado-Peinado, M.; Polášek, M.; Tureček, F. Specific Generation of 1-Methylcytosine Radicals in the Gas-Phase. *Angew. Chem., Int. Ed. Engl.* **2005**, *44*, 6708−6711.
(35) Wee, S.; O'Hair, R. A. J.; McFadyen, W. D. Can Radical Cations of the Constituents of Nucleic Acids Be Formed in the Gas Phase Using Ternary Transition Metal Complexes? *Rapid Commun. Mass Spectrom.* **2005**, *19*, 1797−1805.
(36) Lam, A. K.; Abrahams, B. F.; Grannas, M. J.; McFadyen, W. D.; O'Hair, R. A. J. Tuning the Gas Phase Redox Properties of Copper(II) Ternary Complexes of Terpyridines to Control the Formation of Nucleobase Radical Cations. *Dalton Trans.* **2006**, 5051−5061.
(37) Feketeova, L.; Yuriev, E.; Orbell, J. D.; Khairallah, G. N.; O'Hair, R. A. J. Gas-Phase Formation and Reactions of Radical Cations of Guanosine, Deoxyguanosine and Their Homodimers and Heterodimers. *Int. J. Mass Spectrom.* **2011**, *304*, 74−82.
(38) Feketeova, L.; Chan, B.; Khairallah, G. N.; Steinmetz, V.; Maitre, P.; Radom, L.; O'Hair, R. A. J. Gas-Phase Structure and Reactivity of the Keto Tautomer of the Deoxyguanosine Radical Cation. *Phys. Chem. Chem. Phys.* **2015**, *17*, 25837−25844.
(39) Sun, Y.; Zhou, W.; Moe, M. M.; Liu, J. Reactions of Water with Radical cations of Guanine, 9-Methylguanine, 2′-Deoxyguanosine and Guanosine: Keto-Enol Isomerization, C8 Hydroxylation, and Effects of N9-Substitution. *Phys. Chem. Chem. Phys.* **2018**, *20*, 27510−27522.
(40) Dang, A.; Liu, Y.; Tureček, F. UV-Vis Action Spectroscopy of Guanine, 9-Methylguanine and 2′-Deoxyguanosine Cation Radicals in the Gas Phase. *J. Phys. Chem. A* **2019**, *123*, 3272−3284.
(41) Syka, J. E. P.; Coon, J. J.; Schroeder, M. J.; Shabanowitz, J.; Hunt, D. F. Peptide and Protein Sequence Analysis by Electron Transfer Dissociation Mass Spectrometry. *Proc. Natl. Acad. Sci. U. S. A.* **2004**, *101*, 9528−9533.
(42) Xia, Y.; Gunawardena, H. P.; Erickson, D. E.; McLuckey, S. A. Effects of Cation Charge-Site Identity and Position on Electron-Transfer Dissociation of Polypeptide Cations. *J. Am. Chem. Soc.* **2007**, *129*, 12232−12243.
(43) Hari, Y. I.; Leumann, C.; Schürch, S. What Hinders Electron Transfer Dissociation (ETD) of DNA Cations? *J. Am. Soc. Mass Spectrom.* **2017**, *28*, 2677−2685.
(44) Huang, S. R.; Liu, Y.; Tureček, F. UV-Vis Photodissociation Action Spectroscopy Reveals Cytosine-Guanine Hydrogen Transfer in DNA Tetranucleotide Cation Radicals upon One-Electron Reduction. *J. Phys. Chem. B* **2020**, *124*, 3505−3517.
(45) Liu, Y.; Huang, S. R.; Tureček, F. Guanine-Adenine Interactions in DNA Tetranucleotide Cation Radicals Revealed by UV/Vis Photodissociation Action Spectroscopy and Theory. *Phys. Chem. Chem. Phys.* **2020**, *22*, 16831−16842.
(46) Turecek, F. Flying DNA Cation Radicals in the Gas Phase: Generation and Action Spectroscopy of Canonical and Noncanonical Nucleobase Forms. *J. Phys. Chem. B* **2021**, *125*, 7090−7100.
(47) Vrkic, A. K.; O'Hair, R. A. J.; Foote, S.; Reid, G. E. Fragmentation Reactions of all 64 protonated Trimer Oligonucleotides Via Tandem Mass spectrometry in an Ion Trap. *Int. J. Mass Spectrom.* **2000**, *194*, 145−164.
(48) Wan, J.; Brož, B.; Liu, Y.; Huang, S. R.; Marek, A.; Tureček, F. Resolution of Identity in Gas-Phase Dissociations of Mono and Diprotonated DNA Codons by ^{15}N-Labeling and Computational Structure Analysis. *J. Am. Soc. Mass Spectrom.* **2022**, *33*, 1936−1950.
(49) Brož, B.; Tureček, F.; Marek, A. Low Scale Syringe-Made Synthesis of ^{15}N-Labeled Oligonucleotides. *J. Label. Compd. Radiopharm.* **2022**, *65*, 309−314.
(50) Hartmer, R.; Kaplan, D. A.; Gebhardt, C. R.; Ledertheil, T.; Brekenfeld, A. Multiple Ion/Ion Reactions in the 3D Ion Trap: Selective Reagent Ion Production for ETD and PTR from a Single Compound. *Int. J. Mass Spectrom.* **2008**, *276*, 82−90.
(51) Berendsen, H. J.; Postma, J. V.; van Gunsteren, W. F.; DiNola, A. R. H. J.; Haak, J. R. Molecular Dynamics with Coupling to an External Bath. *J. Chem. Phys.* **1984**, *81*, 3684−3690.
(52) Řezáč, J.; Fanfrlík, J.; Salahub, D.; Hobza, P. Semi-Empirical Quantum Chemical PM6Method Augmented by Dispersion and H Bonding Correction Terms Reliably Describes Various Types of Noncovalent Complexes. *J. Chem. Theory Comput.* **2009**, *5*, 1749−1760.
(53) Stewart, J. J. P. *MOPAC 16*; Stewart Computational Chemistry: 2016.
(54) Řezáč, J. Cuby: An Integrative Framework for Computational Chemistry. *J. Comput. Chem.* **2016**, *37*, 1230−1237.
(55) Becke, A. D. Density-Functional Exchange-Energy Approximation with Correct Asymptotic Behavior. *Phys. Rev. A* **1988**, *38*, 3098−3100.
(56) Grimme, S.; Ehrlich, S.; Goerigk, L. Effect of the Damping Function in Dispersion Corrected Density Functional Theory. *J. Comput. Chem.* **2011**, *32*, 1456−65.
(57) Zhao, Y.; Truhlar, D. G. The M06 Suite of Density Functionals for Main Group Thermochemistry, Thermochemical Kinetics, Noncovalent Interactions, Excited States, and Transition Elements: Two New Functionals and Systematic Testing of Four M06-Class Functionals and 12 Other Functionals. *Theor. Chem. Acc.* **2008**, *120*, 215−241.
(58) Huang, S. R.; Tureček, F. Noncanonical Isomers of Nucleoside Cation Radicals: An Ab Initio Study of the Dark Matter of DNA Ionization. *J. Phys. Chem. A* **2022**, *126*, 2480−2497.
(59) Reed, A. E.; Weinstock, R. B.; Weinhold, F. Natural Population Analysis. *J. Chem. Phys.* **1985**, *83*, 735−746.
(60) Korn, J. A.; Urban, J.; Dang, A.; Nguyen, H. T. H.; Turecek, F. UV-Vis Action Spectroscopy Reveals a Conformational Collapse in Hydrogen-Rich Dinucleotide Cation Radicals. *J. Phys. Chem. Lett.* **2017**, *8*, 4100−4107.
(61) Liu, Y.; Ma, C.; Nováková, G.; Marek, A.; Tureček, F. Charge-Tagged Nucleosides in the Gas Phase: UV-Vis Action Spectroscopy and Structures of Cytidine Cations, Dications, and Cation Radicals. *J. Phys. Chem. A* **2021**, *125*, 6096−6108.
(62) Liu, Y.; Ma, C.; Leonen, C. J. A.; Chatterjee, C.; Nováková, G.; Marek, A.; Tureček, F. Tackling a Curious Case. Generation of Charge-Tagged Guanosine Radicals by Electron Transfer in the Gas Phase and Their Characterization by UV-Vis Photodissociation Action Spectroscopy and Theory. *J. Am. Soc. Mass Spectrom.* **2021**, *32*, 772−785.
(63) Holm, A. I. S.; Larsen, M. K.; Panja, S.; Hvelplund, P.; Nielsen, S. B.; Leib, R. D.; Donald, W. A.; Williams, E. R.; Hao, C.; Tureček, F. Electron Capture, Femtosecond Electron Transfer and Theory: A Study of Noncovalent Crown Ether 1, *n*-Diammonium Alkane Complexes. *Int. J. Mass Spectrom.* **2008**, *276*, 116−126.
(64) Viglino, E.; Lai, C. K.; Mu, X.; Chu, I. K.; Tureček, F. Ground and Excited-Electronic State Dissociations of Hydrogen-Rich and Hydrogen-Deficient Tyrosine Peptide Cation Radicals. *J. Am. Soc. Mass Spectrom.* **2016**, *27*, 1454−1467.
(65) Gunawardena, H. P.; He, M.; Chrisman, P. A.; Pitteri, S. J.; Hogan, J. M.; Hodges, B. D.; McLuckey, S. A. Electron Transfer versus Proton Transfer in Gas-Phase Ion/Ion Reactions of Polyprotonated Peptides. *J. Am. Chem. Soc.* **2005**, *127*, 12627−12639.
(66) McLuckey, S. A.; Van Berkel, G. J.; Glish, G. L. Tandem Mass Spectrometry of Small, Multiply Charged Oligonucleotides. *J. Am. Soc. Mass Spectrom.* **1992**, *3*, 60−70.
(67) Murray, K. K. DNA Sequencing by Mass Spectrometry. *J. Mass Spectrom.* **1996**, *31*, 1203−1215.
(68) Schürch, S. Characterization of Nucleic Acids by Tandem Mass Spectrometry-The Second Decade (2004−2013): From DNA to RNA and Modified Sequences. *Mass Spectrom. Rev.* **2016**, *35*, 483−523.
(69) Tureček, F.; Yao, C. Hydrogen Atom Addition to Cytosine, 1-Methylcytosine, and Cytosine-Water Complexes. A Computational

https://doi.org/10.1021/jasms.2c00322
J. Am. Soc. Mass Spectrom. 2023, 34, 304−319

Study of a Mechanistic Dichotomy. *J. Phys. Chem. A* **2003**, *107*, 9221−9231.
(70) Chen, X.; Syrstad, E. A.; Nguyen, M. T.; Gerbaux, P.; Tureček, F. Adenine Radicals in the Gas Phase. An Experimental and Computational Study of Hydrogen Atom Adducts to Adenine. *J. Phys. Chem. A* **2005**, *109*, 8121−8132.
(71) Wu, R. R.; Hamlow, L. A.; He, C. C.; Nei, Y. W.; Berden, G.; Oomens, J.; Rodgers, M. T. The Intrinsic Basicity of the Phosphate Backbone Exceeds that of Uracil and Thymine Residues: Protonation of the Phosphate Moiety is Preferred over the Nucleobase for pdThd and pUrd. *Phys. Chem. Chem. Phys.* **2017**, *19*, 30351−30361.
(72) Rodgers, M. T.; Campbell, S.; Marzluff, E. M.; Beauchamp, J. L. Site-Specific Protonation Directs Low-Energy Dissociation Pathways of Dinucleotides in the Gas Phase. *Int. J. Mass Spectrom. Ion Processes* **1995**, *148*, 1−23.
(73) Tureček, F.; Gu, M.; Hop, C. E. C. A. Franck-Condon Dominated Chemistry. Formation and Dissociations of Tetrahydroxyphosphoranyl Radicals Following Femtosecond Reduction of Their Cations in the Gas Phase. *J. Phys. Chem.* **1995**, *99*, 2278−2291.

https://doi.org/10.1021/jasms.2c00322
J. Am. Soc. Mass Spectrom. 2023, 34, 304−319